I. Gas Phase Proton Affinity of Zwitterionic Betaine

II. High Resolution Spectroscopy of Trapped Ions: Concept and Design

Thesis by

Hak-No Lee

In Partial Fulfillment of the Requirements

for the Degree of

Doctor of Philosophy

California Institute of Technology

Pasadena, California

1999

(Submitted September 30, 1998)

Acknowledgements

Much gratitude is owed to my thesis advisors, Professors Jack Beauchamp and Dan Weitekamp, for their guidance and support. I feel fortunate to have worked with advisors who value and emphasize the training of their students. I thank them for allowing me to pursue studies of my own interest, without the pressure to produce timely results. Such freedom has enabled me to obtain exposure to a wide variety of areas in physical chemistry and chemical physics: An invaluable training that would be difficult to attain after graduation.

There are many people whose support and friendship enriched my years at Caltech, including fellow graduate students and the staff of the chemistry department. Special thanks go to the members of Beauchamp group, past and present: Sherrie Campbell, Elaine Marzluff, Kevin Crellin, Jim Smith, Sang Won Lee, Dmitri Kossakovski, Hyun Sik Kim, Thomas Schindler, Patrick Vogel, and Priscilla Boon. Always willing to help and answer questions, they contributed significantly to my learning and provided companionship for which I am grateful.

Abstract

In an ideal experiment, the system being investigated is isolated from the environment. The only external influences allowed on the system are the parameters that the experimenter chooses to vary, in effort to study their effects on the observables. Moreover, these parameters can be controlled with all the accuracy and precision desired by the experimenter. In chemistry, ion cyclotron resonance (ICR) mass spectrometry may come closer to replicating this ideal condition than any other experimental technique. An ion isolated in an ICR trap is under ultra high vacuum, devoid of physical contact with other atomic and molecular systems, as well as with the apparatus itself. Confined to a small volume and for a practically unlimited length of time, its few connections with the external environment, such as temperature and the electric and magnetic trapping fields, are well under the experimenter's control. And since the motion of a charged particle in electric and magnetic fields is completely known, the ion can be manipulated with an unequaled freedom and certainty. In this dissertation, two experimental methods which utilize these unique capabilities of ICR spectrometry are explored.

In Chapter 1, the kinetic method is applied to determine the gas phase proton affinity of the zwitterion betaine, $(CH_3)_3N^+CH_2CO_2^-$. Protonated dimers of betaine with reference bases of known proton affinities are formed by Cs^+ bombardment of a glycerol solution in an external ion source FT-ICR. Product distributions resulting from off-

resonance collisional activation of isolated adducts are analyzed to yield a value of 242 ± 1 kcal/mol for the gas phase proton affinity of betaine. This is 103 kcal/mol less than that of the isoelectronic *tert*-butylacetate anion, $(CH_3)_3CCH_2CO_2^-$, and the difference can be attributed to the electrostatic dipolar stabilization of the carboxylate anion in betaine. In addition, a general analysis of the kinetic method is presented based on RRKM unimolecular reaction theory. This analysis does not assume a Boltzmann distribution of internal energies in the reactant ion and provides a rationalization for the success of the method even when different experimental techniques are used.

While ICR has proven to be a powerful technique for studying the chemical properties of gas phase ions, it suffers from a serious weakness which prevents full realization of its unique capabilties: The only observable it measures is the mass. This has kept ICR from being widely used to investigate the physical properties of molecular ions. In Chapter 2, a novel method for obtaining high-resolution r.f. and microwave spectra of ions in ICR trap is proposed. Termed *i*nternally *r*esonant *i*on *t*rapping *e*xcitation (IRITE), it uses spatially inhomogeneous a.c. electric fields to couple the internal energy states with the ion's translation motion. The resonance absorption of radiation is detected by its effect on the oscillations of the trapped ions, rather than on the radiation. The theoretical concept behind IRITE is introduced, and an experiment designed to demonstrate its feasibility by observing r.f. transitions in HCl^+ is discussed in details. Combined with ICR's unsurpassed ability to isolate and manipulate chemical systems, this new technique promises to allow chemists to study phenomena previously unobservable even in neutral molecules.

Table of Contents

List of Figures

Chapter 1: Gas Phase Proton Affinity of Zwitterionic Betaine

1.1 Introduction

In many complex organic and biological systems, the chemistry of functional groups is believed to be influenced by the electrostatic field of a nearby charge center. This effect is expected to be particularly significant if the chemistry involves charged intermediates. For example in most enzymatic reactions, where the donation or abstraction of a hydrogen ion is a critical step,[1] stabilization of the intermediates by oppositely charged side chains of nearby amino acid residues is assumed to play a major role in the catalytic mechanisms and the lowering of reaction barriers. Although the importance of such dipolar stabilization is well recognized, there are no previous experimental studies of this electrostatic effect in an isolated system. Difficulty in discerning the diminished electrostatic effect from other interactions complicates the quantitative interpretation of such experiments in solution phase. In the gas phase, where charge formation is highly unfavorable energetically, the difficulty lies in finding appropriate model systems. In this investigation, we identify such a model system, betaine (figure 1.1a),[2] and describe an experimental determination of the electrostatic effect on its proton affinity.

Protonated betaine is an isoelectronic analog of *tert*-butylacetic acid (figure 1.1b).[2] The carboxyl groups of the two compounds are identical except for the electrostatic and

a.

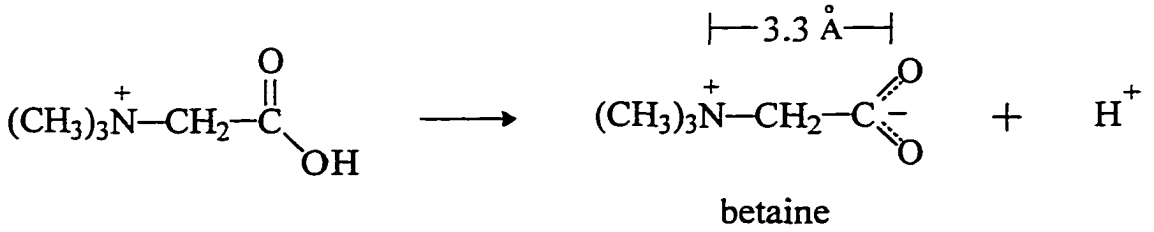

betaine

b.

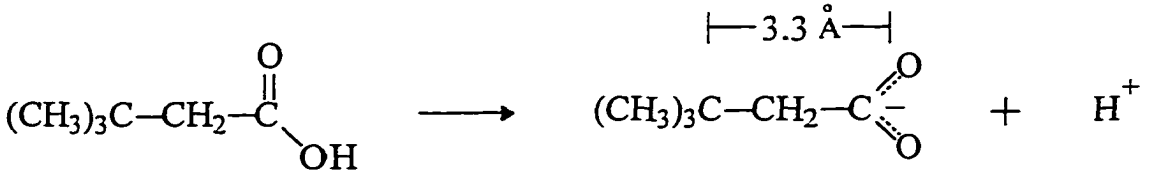

t-butylacetic acid

Figure 1.1: (a) Acid dissociation of protonated betaine. 3.3 Å is the average of the distances between the nitrogen and the oxygens (2.9 and 3.7 Å).[2] (b) Acid dissociation of *t*-butylacetic acid. The distances between the tertiary carbon and the oxygens are 3.0 and 3.6 Å.[2] Proton affinity is defined as $E_{PA} = -\Delta H_{rxn}$.

the electronic induction (i.e., withdrawing of electrons through the bonds) effects of the localized positive charge in betaine. As discussed below, the electronic induction effect is much smaller than the electrostatic effect in the gas phase. Thus the difference between proton affinities of the two compounds is a measure of the electrostatic effect that a positive charge 3.3 Å away has on the acidity of a carboxylic acid group.

Gas phase proton affinities are ordinarily determined by measuring the proton-transfer equilibrium between the compound under investigation and a reference compound of known proton affinity.[3] The proton affinity of *t*-butylacetate anion, 344.9 ± 2.1 kcal/mol,[4] has been determined by this equilibrium method. However, the technique is not applicable to non-volatile compounds like betaine. In such cases the kinetic

method developed by Cooks and co-workers[5] provides a viable alternative. The kinetic method relies on the competitive dissociations of weakly-bound cluster ions to measure thermochemical properties. For example, to determine the proton affinity of compound A,

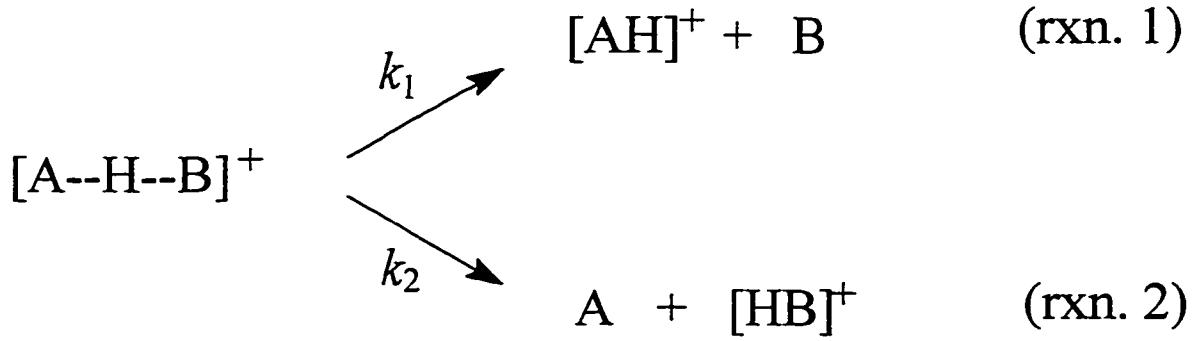

a protonated adduct formed between A and a reference compound B of known proton affinity is collisionally dissociated. These experiments have shown a simple relationship between the product ion populations and the proton affinities, E_{PA}, of A and B:

$$\ln\left\{\frac{I_{[AH]^+}}{I_{[HB]^+}}\right\} = C + C'\left[E_{PA}(A) - E_{PA}(B)\right] . \qquad [1.1]$$

$I_{[AH]^+}/I_{[HB]^+}$ is the ratio of the product ion populations, and C and C' are constants for a given set of experimental conditions. $E_{PA}(A)$ is typically determined by using a series of different reference compounds of similar E_{PA}. The method is quite general, and the competitive dissociation of appropriate adducts can be used to determine other thermochemical properties, such as metal ion affinities and electron affinities.[6]

Since its introduction in 1977,[5] the kinetic method has been successfully applied to a wide variety of systems, and its application has grown in recent years with increasing

research activities in the gas phase study of biomolecules.[7-9] However, the often invoked theoretical model behind the kinetic method (i.e., rationalization of eqn. 1.1), which is based on the transition state theory, suffers from well-recognized deficiencies.[5,8,10] Recently, a more appropriate rationalization based on RRK unimolecular reaction theory has been proposed,[8] and in this article we expand on these efforts by providing a more general RRKM analysis of the kinetic method.

1.2 Experimental Section

Collision-induced dissociation (CID) experiments were performed using an external ion source Fourier transform ion cyclotron resonance (FT-ICR) mass spectrometer, built in cooperation with IonSpec Corporation (Irvine, CA). A detailed description of this instrument has been previously published.[11] The spectrometer is equipped with an external Cs^+ bombardment source and an octopole ion guide for transferring ions into the 2 × 2 × 3 in. reaction cell, which is located in the high field region of the superconducting magnet (7 T). A split injection electrode at the entrance of the ICR cell provides for efficient trapping of the transferred ions.[12] The instrument has three regions of differential cryogenic pumping, resulting in a residual background pressure of ~5×10^{-10} Torr in the cell. An accurate pressure measurement is achieved by calibrating a specially designed ionization gauge[13] attached directly on the reaction cell with a capacitance manometer connected to the cell through a static port. For the experiments reported here, a static pressure of N_2 (2.0×10^{-7} Torr) was maintained in the cell for use as collision gas.

All chemicals were purchased from commercial suppliers and used as received. Betaine monohydrate and trifluoroacetic acid were purchased from Sigma Chemical (St. Louis, MO) and EM Science (Gibbstown, NY), respectively. All other compounds were obtained from Aldrich Chemical (Milwaukee, WI). The reference bases used in the experiments are shown in figure 1.2.[14,15]

Samples were prepared by mixing 0.1 mL glycerol, 30 mg betaine monohydrate, 30 μL trifluoroacetic acid, and 30 μL of the reference base. Approximately 5 μL of this solution was applied to the probe tip for each experiment. Ions were generated by bombarding the sample with fast Cs^+ ions (6-8 keV) and transported to the cell (1.8 V trapping potential) using the octopole ion guide (50–150 volts, ~1.2 MHz) and the split electrode injection (~6 V differential). Ions other than the species of interest (protonated betaine-reference base adducts) in the 50 to 450 *m/z* range were ejected, and the adduct ions were then translationally excited with a radio frequency (r.f.) pulse slightly off-resonant from their cyclotron frequency (1.5–2.0 kHz lower);[16] causing them to undergo multiple collisions with the N_2 gas and gradually accumulate internal energy. The pulse strength was varied to control the average energy per collision (0.1–1.8 eV in the center-of-mass frame). Depending on the reference base used, 1.1 eV to 1.5 eV was enough to dissociate >90% of the dimers with 0.5 second of irradiation. Resulting ions in the 35–450 *m/z* range were detected, and this time-domain signal (32.8 ms, 256 kilobytes) was digitized and saved on the computer for later processing. The signals from 10–20 scans were averaged and Fourier transformed to the frequency-domain to provide the mass spectrum.

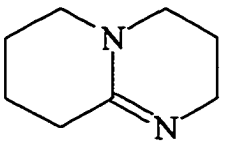

1,8-Diazabicyclo [5.4.0] undec-7-ene
(DBU)
PA 247.5 kcal/mol

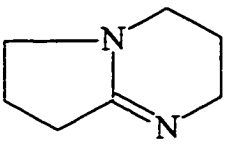

1,5-Diazabicylco [4.3.0] non-5-ene
(DBN)
PA 245.1 kcal/mol

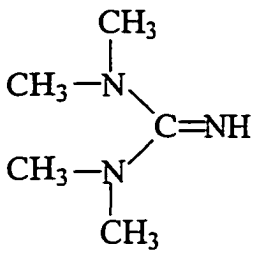

1,1,3,3-Tetramethylguanidine
(TMG)
PA 243.1 kcal/mol

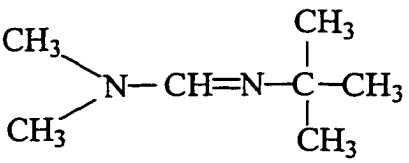

N'-*tert*-Butyl-N,N-Dimethylformamidine
(BDF)
PA 240.8 kcal/mol

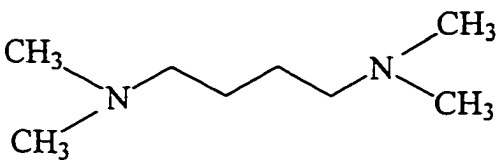

N,N,N',N'-Tetramethyl-1,4-butanediamine
(TMBDA)
PA 240.8 kcal/mol

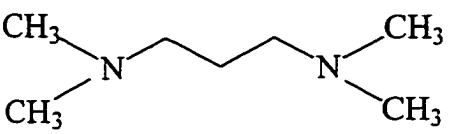

N,N,N',N'-Tetramethyl-1,3-Propanediamine
(TMPDA)
PA 239.6 kcal/mol

Figure 1.2: Structures and proton affinities (PA) of the reference bases used in the kinetic method experiments.[14,15] Not shown is tri-*n*-butylamine (TBA) with PA 236.0 kcal/mol.

1.3 Theory

1.3.a Transition State Theory of the Kinetic Method. The kinetic method is most often analyzed using transition state theory;

$$k(T) = \frac{RT}{h}\frac{Q^*}{Q}e^{-E_a/RT}, \qquad [1.2]$$

where Q is the partition function of the adduct ion, Q^* is that for the transition state, and E_a is the activation energy. For a reaction with only two competing channels, the rate constants k_1 and k_2 determine the relative abundances of the dissociation products, $[AH]^+$ and $[BH]^+$:

$$\frac{I_{[AH]^+}}{I_{[HB]^+}} = \frac{k_1}{k_2}. \qquad [1.3]$$

Then

$$\ln\left[\frac{I_{[AH]^+}}{I_{[HB]^+}}\right] = \ln\left[\frac{k_1(T)}{k_2(T)}\right] = \ln\left[\frac{Q_1^*Q_2}{Q_2^*Q_1}\right] - \frac{\Delta E_a}{RT} \qquad [1.4]$$

with $\Delta E_a = E_a^{(1)} - E_a^{(2)}$. The reactions proceed from the same reactant, $Q_1 = Q_2$, and transition states of the two reaction pathways differ most significantly by the vibrational frequencies of the remaining bonds to the proton, $Q_1^*/Q_2^* \approx \nu(A\cdots H^+)/\nu(B\cdots H^+) = \nu_1/\nu_2$:[5]

$$\ln\left[\frac{I_{[AH]^+}}{I_{[HB]^+}}\right] = \ln\left[\frac{k_1(T)}{k_2(T)}\right] \approx \ln\left[\frac{\nu_1}{\nu_2}\right] - \frac{\Delta E_a}{RT}. \qquad [1.5]$$

It is usually assumed that the ratio ν_1/ν_2 does not vary much and remains constant[5,7] when different reference compounds of similar $E_a^{(2)}$ are used.

The difference in activation energies of the two reactions, ΔE_a, can be equated to the difference between proton affinities, $E_{PA}(A) - E_{PA}(B)$, if the following two conditions

are satisfied. (1) If the reference compounds B are chosen so that they are structurally similar to A, then the two reaction pathways should have similar entropy changes, and (2) since the reactions are simple dissociations, there will be negligible barriers for the reverse reactions. Under these situations, a plot of $\ln[I_{[AH]^+}/I_{[HB]^+}]$ vs. $E_{PA}(B)$ obtained using a series of reference compounds will result in a straight line of slope $-1/RT$. $E_{PA}(A)$ is determined from the point on the line where $\ln[I_{[AH]^+}/I_{[HB]^+}] = 0$. The possibility of an error being introduced by the approximations, in particular the neglect of entropy changes, is minimized by utilizing a large number of reference compounds.

As mentioned in the introduction, many successful applications of the kinetic method have been reported. Yet the rationalization of the method based on transition state theory suffers from a fundamental weakness which prevents a full understanding of its limits and utility. For transition state theory to be pertinent, the reacting ions, $[A\text{--}H\text{--}B]^+$, must be in thermal equilibrium. But the actual experimental conditions, in which isolated ions undergo metastable and collision-induced dissociations, clearly prohibit the reacting ions from attaining a Boltzmann distribution of internal energies.[5,8,10] A proper analysis of the kinetic method requires microcanonical reaction rate theories which avoid reference to a thermodynamic temperature.

1.3.b RRK Theory of the Kinetic Method. Campbell *et al.*[8] offered a rationalization of the kinetic method based on RRK unimolecular reaction theory. This is reviewed here, since useful comparisons can be made between this and the RRKM analysis presented below.

The expression for the classical RRK rate constant is[17]

$$k(E) = \nu\left(\frac{E - E_o}{E}\right)^{s-1}, \qquad [1.6]$$

where ν is the frequency factor for the reaction, E is the total internal excitation of the reactant molecule with s vibrational degrees of freedom, and E_o is the critical energy for the reaction. For the two competing reaction channels,

$$\frac{k_1(E)}{k_2(E)} = \frac{\nu_1}{\nu_2}\left(\frac{E - E_1}{E - E_2}\right)^{s-1}, \qquad [1.7]$$

where E_1 and E_2 are the critical energies for rxn. 1 and rxn. 2, respectively. Manipulation of eqn. 1.7 yields

$$\ln\left[\frac{k_1(E)}{k_2(E)}\right] = \ln\left(\frac{\nu_1}{\nu_2}\right) + (s-1)\ln\left(\frac{E - E_1}{E - E_2}\right). \qquad [1.8]$$

Provided that $|E_2 - E_1|$ is small compared to $E - E_1$,[8]

$$\ln\left[\frac{k_1(E)}{k_2(E)}\right] \approx \ln\left(\frac{\nu_1}{\nu_2}\right) - (s-1)\left(\frac{E_2 - E_1}{E - E_1}\right). \qquad [1.9]$$

This is an appropriate approximation under the experimental conditions of the kinetic method. For dissociation products to be detectable using FT-ICR mass spectrometer, ions must fall apart on a time scale less than 1 sec, corresponding to reaction rates greater than 1 sec^{-1}. Other mass spectrometry techniques involve time scales that are narrow in range. For dissociation products to be detectable in a sector instrument, for example, ions must dissociate at rates between 10^4 sec^{-1} and 10^5 sec^{-1}. According to RRKM calculations, these rates may require the excess energy $E - E_1$ to be several times that of the barrier height for large ions. Since the strength of an ionic hydrogen bond in the gas phase between two compounds of similar proton affinities is between 20 and 30 kcal/mol,[18] the

condition $|E_2 - E_1| << E - E_1$ is fulfilled by employing reference compounds whose proton affinities do not differ greatly from that of the compound under investigation.

With the two assumptions described in the transition state theory derivation that equate $E_1 - E_2$ with the difference between the proton affinities of A and B, eqn. 1.9 becomes

$$\ln\left[\frac{k_1(E)}{k_2(E)}\right] \approx \ln\left(\frac{\nu_1}{\nu_2}\right) - (s-1)\left[\frac{E_{PA}(\mathrm{B}) - E_{PA}(\mathrm{A})}{E - E_1}\right]. \qquad [1.10]$$

The ratio ν_1/ν_2 is again presumed to remain relatively constant with different reference compounds of similar E_{PA}, and eqn. 1.10 correctly predicts the straight line in the plot, $\ln[I_{[AH]+}/I_{[HB]+}]$ vs. $E_{PA}(B)$. Moreover, according to eqn. 1.10, the inverse of the slope of the plot is equal to the excess internal energy per degree of freedom in the activated complex;

$$|\mathrm{slope}|^{-1} = \frac{E - E_1}{s-1}. \qquad [1.11]$$

This helps to explain why the kinetic method works regardless of the size and, within reasonable limits, the structure of the reference compounds used. The temporal constraint of the different experimental methods selects reactants which have the same excess energy per vibrational degree of freedom. The method of excitation is irrelevant, as long as it produces a distribution of internal excitation which includes the energy required to dissociate the ions at the necessary rate. RRKM calculations have shown that, for similar frequency factors and barrier heights, dissociation rates for systems of varying size are approximately the same when the excess energies per vibrational degree of freedom in the activated complexes are comparable.[8]

1.3.c RRKM Theory of the Kinetic Method. In RRK theory a molecule is modeled as a system of loosely coupled harmonic oscillators. When compared to experimental values, k(E) in RRK theory can sometimes be off by an order of magnitude or more. In this section, RRKM unimolecular reaction theory is utilized to rationalize the kinetic method. This analysis does not depend on a specific model for the active modes in the reacting ion and the transition state, which makes it more applicable to realistic systems.

The RRKM rate constant can be written as[17,19]

$$k(E) = \frac{G^{\ddagger}(E - E_o)}{hN(E)} , \qquad [1.12]$$

where $G^{\ddagger}(E - E_o)$ is the sum of states for the active degrees of freedom in the transition state, h is the Planck's constant, and $N(E)$ is the density of states for the active degrees of freedom in the reacting ion. The desired ratio of rate constants is then equal to ratio of the sums of states for the transition states:

$$\frac{k_1(E)}{k_2(E)} = \frac{G_1(E - E_1)}{G_2(E - E_2)} . \qquad [1.13]$$

The densities of states of the reactant for the two reactions cancel out, since they are equal according to the rapid intramolecular energy transfer assumption of RRKM theory.

The sum of states is usually expressed semi-classically in terms of a phase-space volume integral,[17,19]

$$G(E) = \frac{1}{h^S} \int \cdots \iint_{H=E} \prod_{i=1}^{S} dq_i dp_i , \qquad [1.14]$$

with the Hamiltonian of the system as the constraint. For the derivation of the kinetic method to be general, the potential of the Hamiltonian cannot be specified, and converting eqn. 1.14 into a useful expression is a difficult task. Forst gives another semiclassical equivalent of eqn. 1.14:[19]

$$G(E) = \int \cdots \iint_{f(n_i) \le E} \prod_{i=1}^{S} g_i dn_i \ , \qquad [1.15]$$

where n_i is the quantum number for the i-th degree of freedom and g_i is the degeneracy associated with n_i. The constraint (i.e., the energy) is a continuous function of n_1, n_2, n_3, ... n_s. In RRKM theory, the degrees of freedom are assumed independent and separable. Then the function $f(n_i)$ can usually be written in the form,[19]

$$f(n_i) = \sum_{i=1}^{S} \left(\frac{n_i}{a_i} \right)^{p_i} , \qquad [1.16]$$

where a_i and p_i are constants. Forst's representations, eqns. 1.15 and 1.16, are not particularly useful when calculating an actual value for the sum of states, since energy is considered as a continuous function. Even for the large systems that the kinetic method is typically used to investigate, the approach is expected to be unsuitable. However, if a_i and p_i are treated as empirical parameters, then an accurate number for $G(E)$ can be obtained.[19] This requires appropriate values for a and p of each mode to be known, but for the purpose at hand it is sufficient to recognize that eqn. 1.15 can represent the actual sum of states.

Eqn. 1.15 with the constraint $f(n_i) \le E$ is a Dirichlet's integral, whose solution is[20]

$$G(E)=\prod_{i=1}^{s}\left[\frac{a_i^{m_i}\,\Gamma\left(m_i/p_i\right)}{p_i}\right]\cdot\frac{E^{\sum_{i=1}^{s}\frac{m_i}{p_i}}}{\Gamma\left(1+\sum_{i=1}^{s}m_i/p_i\right)}, \qquad [1.17]$$

where $\Gamma(z)$ are gamma functions and $m_i - 1$ equals the exponent of the quantum number in the degeneracy g_i. For example, $m_i = 1$ if the i-th mode is a harmonic oscillator, since g_i is independent of quantum number. The ratio of sums of states for the two transition states is

$$\frac{G_1(E-E_1)}{G_2(E-E_2)}=\prod_{i=2}^{s}\left[\frac{a_i^{m_i}\Gamma\left(m_i/p_i\right)}{p_i}\right]\cdot\prod_{\substack{j=1\\ \neq 2}}^{s}\left[\frac{p_j}{a_j^{m_j}\Gamma\left(m_j/p_j\right)}\right]\cdot\frac{\Gamma\left(1+\sum_{\substack{j=1\\ \neq 2}}^{s}m_j/p_j\right)}{\Gamma\left(1+\sum_{i=2}^{s}m_i/p_i\right)}\cdot\frac{\left(E-E_1\right)^{\sum_{i=2}^{s}\frac{m_i}{p_i}}}{\left(E-E_2\right)^{\sum_{\substack{j=1\\ \neq 2}}^{s}\frac{m_j}{p_j}}}. \qquad [1.18]$$

Eqn. 1.18 is written with the i=1 and j=2 modes designated as the reaction coordinates of the transition states for rxn. 1 and rxn. 2, respectively:

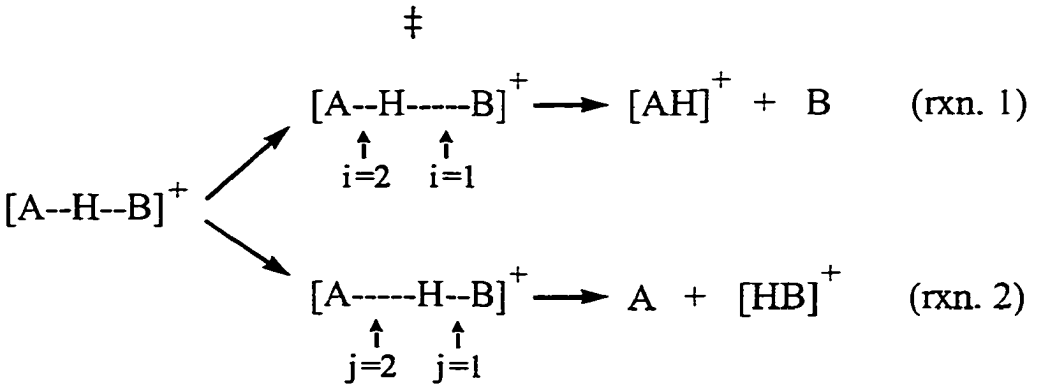

To make further progress from eqn. 1.18, an assumption regarding the transition states must be made: for a weakly bonded complex going through a simple dissociation, the two transition states are similar except for the modes involved in the breaking of the hydrogen bond;

$$a_i \cong a_j \;;\quad p_i \cong p_j \;;\quad m_i = m_j \qquad \text{for } i = j \neq 1 \text{ or } 2\ . \tag{1.19}$$

Then,

$$\frac{G_1(E-E_1)}{G_2(E-E_2)} = \frac{\left(a_{i=2}\right)^{m_{i=2}} p_{j=1}\Gamma\left(m_i/p_{i=2}\right)}{\left(a_{j=1}\right)^{m_{j=1}} p_{i=2}\Gamma\left(m_j/p_{j=1}\right)} \cdot \frac{\Gamma\left(1+\sum_{\substack{j=1\\ \neq 2}}^{s} m_j/p_j\right)}{\Gamma\left(1+\sum_{i=2}^{s} m_i/p_i\right)} \cdot \frac{\left(E-E_1\right)^{\sum_{i=2}^{s} \frac{m_i}{p_i}}}{\left(E-E_2\right)^{\sum_{\substack{j=1\\ \neq 2}}^{s} \frac{m_j}{p_j}}} \tag{1.20}$$

If the two modes involved in the bond breakage are of the same variety (i.e., hydrogen bonds), then

$$p_{i=2} \cong p_{j=1} \; ; \quad m_{i=2} = m_{j=1} \; . \qquad [1.21]$$

No assumptions are required for the relative energies of the modes or their quantum numbers. The validity of this approximation is readily apparent if a physical model is specified for the modes (see below).

The ratio of rate constants can now be expressed as

$$\frac{k_1(E)}{k_2(E)} = \frac{G_1(E-E_1)}{G_2(E-E_2)} \cong \left(\frac{a_2}{a_1}\right)^m \cdot \left(\frac{E-E_1}{E-E_2}\right)^P \qquad [1.22]$$

with

$$m = m_{i=2} = m_{j=1} \; ; \qquad P = \sum_{i=2}^{S} \frac{m_i}{p_i} \cong \sum_{\substack{j=1 \\ \neq 2}}^{S} \frac{m_j}{p_j} \; ; \qquad [1.23]$$

or

$$\ln\left[\frac{k_1(E)}{k_2(E)}\right] \cong m \cdot \ln\left(\frac{a_2}{a_1}\right) + P \cdot \ln\left(\frac{E-E_1}{E-E_2}\right) \; . \qquad [1.24]$$

With $|E_2 - E_1|$ small compared to $E - E_1$,

$$\ln\left[\frac{k_1(E)}{k_2(E)}\right] \approx m \cdot \ln\left(\frac{a_2}{a_1}\right) - P\left(\frac{E_2-E_1}{E-E_1}\right), \qquad [1.25]$$

and

$$\ln\left\{\frac{I_{[AH]^+}}{I_{[HB]^+}}\right\} \approx m \cdot \ln\left(\frac{a_2}{a_1}\right) - P\left\{\frac{E_{PA}(B) - E_{PA}(A)}{E-E_1}\right\} \; . \qquad [1.26]$$

Eqn. 1.26 gives the desired linear relationship between the logarithm of the product ion ratio and the difference in proton affinities, provided that the ratio a_2/a_1 do not vary much with different reference compounds. This would be similar to the assumption made

regarding the frequency factor ratios in the RRK and the transition state theory analyses, but not necessary equivalent since the physical signification of a_i has not been specified.

It is instructive to consider the case when physical models for the active modes are used to express $f(n_i)$ in eqn. 1.16. In RRKM calculations of rate constants, the sum of states $G^*(E-E_o)$ is determined by treating the vibrational degrees of freedom as harmonic oscillators and any internal rotational degrees of freedom as free rotors.[17,19] In such a case, $f(n_i)$ is the sum of the energies of harmonic oscillators and free rotors:

$$f(n_i) = \sum_{i=1}^{r} n_i h\nu_i + \sum_{i=r+1}^{s-1} n_i(n_i+1)\frac{\hbar^2}{2I_i}, \qquad [1.27]$$

where r is the number of the harmonic oscillators and I_i is the moment of inertia of the i-th rotor. The zero-point energy is included in E_o. Then $a_i = (h\nu_i)^{-1}$ for $1 \le i \le r$; $a_i = 2I_i/\hbar^2$ for $r+1 \le i \le s-1$; and $m_i/p_i = 1$ for all i.[19] For simple dissociations of proton-bound dimers, the two modes involved in the bond formation/dissociation are better treated as harmonic oscillators. Then, eqn. 1.26 becomes identical to the expression arrived using the RRK theory, eqn. 1.10:

$$\ln\left\{\frac{I_{[AH]^+}}{I_{[HB]^+}}\right\} \approx \ln\left(\frac{\nu_1}{\nu_2}\right) - (s-1)\left\{\frac{E_{PA}(B) - E_{PA}(A)}{E - E_1}\right\}. \qquad [1.28]$$

1.4 Results and Discussion

As examples, the data obtained using tetramethylguanidine (TMG) as the reference compound are exhibited in figures 1.3(a)–(c). Figure 1.3(a) is a spectrum of the betaine/TMG mixture, and 1.3(b) is that of the isolated adduct after other ions are ejected. Off-resonance collision activation of the adduct gives the product distribution shown in 1.3(c). Table 1 summarizes the results of CID experiments, and the gas phase proton affinity of betaine is determined as 242 kcal/mol from the plot in figure 1.4. Measurements made using this technique have an average uncertainty of ±1 kcal/mol.[8] Analysis of slope of the plot using eqn. 1.11 yields 1.5 kcal/mol of average excess energy per degree of freedom in the activated complex.

In the range of collision energy examined in this investigation (0.1–1.8 eV per collision in the center-of-mass-frame), the CID product ratio was independent of the energy for all of the betaine-base adduct species.[7] The only energy-dependent process observed was the secondary fragmentation of the protonated TMBDA product. Starting at the collision energy of 0.4 eV, a peak with *m/z* of 100.113 appeared in the betaine-TMBDA spectra (figure 1.5a), whose relative intensity rose with increasing energy while the protonated TMBDA peak intensity decreased. The sum of intensities for the two peaks, however, did not vary relative to that of betaine peak (figure 1.6). A CID experiment on protonated TMBDA verified the origin of the new peak, and the identity of ion corresponding to the peak has been tentatively assigned as *N,N*-dimethylpyrrolidine

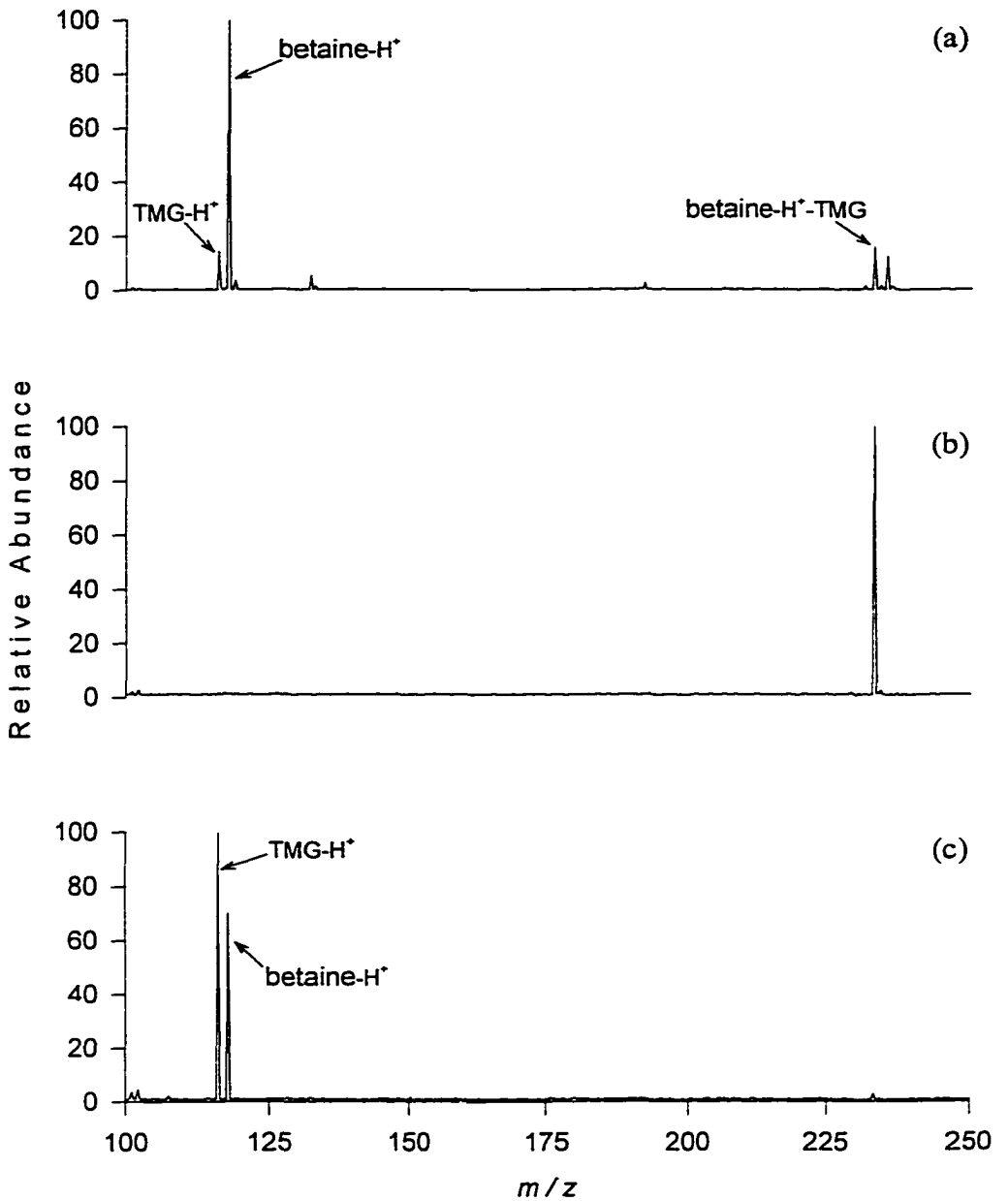

Figure 1.3: (a) Mass spectrum of betaine/TMG mixture. (b) Spectrum of proton-bound betaine-TMG adduct after all other ion species, including the ^{13}C ions, were ejected from the reaction cell. (c) Result of collision-induced dissociation (CID) of the isolated betaine-TMG adduct at average collision energy of 1.3 eV in the center-of-mass frame.

Reference Base	Proton Affinity (kcal/mol)	CID Product Ratio (Betaine-H^+/Base-H^+)
TBA	236.0	27.25
TMPDA	239.6	5.04
TMBDA	240.8	2.27
BDF	240.8	1.63
TMG	243.1	0.69
DBN	245.1	0.11
DBU	247.5	0.02

Table 1.1: Summary of the ratios of product ion populations from the collision-induced dissociations (CID) of proton-bound adducts containing betaine and various reference bases. See figure 1.2 for structures of the bases.

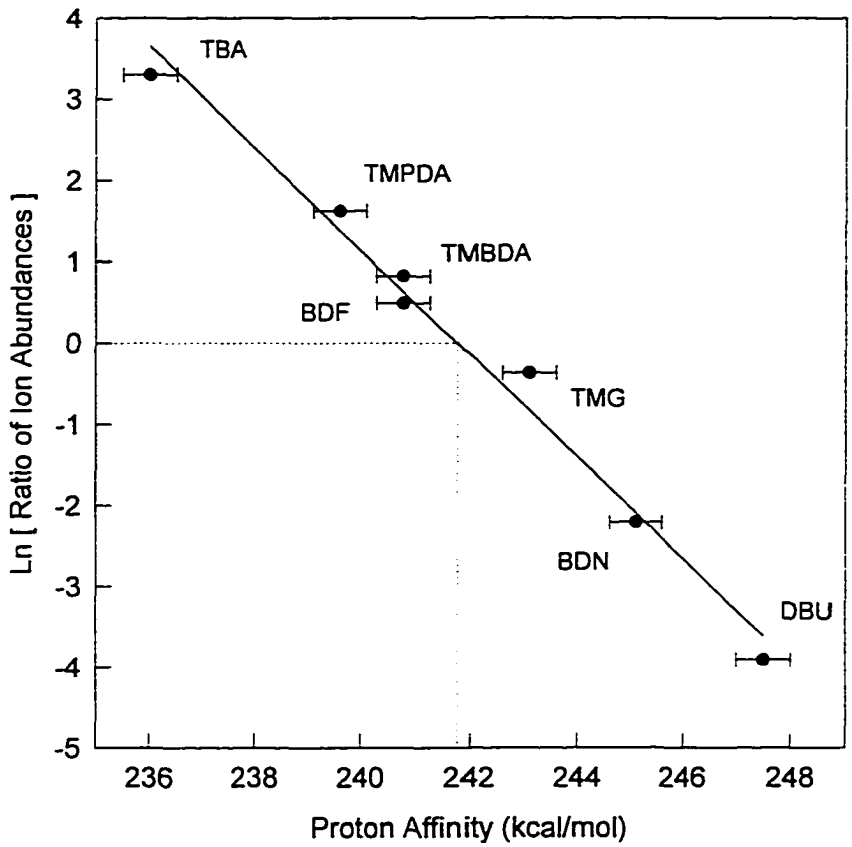

Figure 1.4: Natural logarithm of the ratio of CID products (protonated betaine/protonated reference base) versus reference base proton affinity for seven proton-bound adducts. The proton affinity of betaine extracted from the plot is 242 kcal/mol. Data for these experiments are found in Table 1.1.

cation (DMPC; figure 1.5b). This was the only system to exhibit any significant amount of secondary fragmentation in the energy range examined.

Formation of zwitterions as small as betaine has previously been considered to be too unfavorable energetically to occur in the gas phase.[21,22] Although only *protonated* betaine and bases were actually detected in the experiments, the appearance of protonated bases from the dissociation of the betaine-base adduct is an indication that betaine in its zwitterion form was produced. However, once the free zwitterion is formed, it may subsequently isomerize to *N,N*-dimethylglycine methyl ester, $(CH_3)_2NCH_2COOCH_3$. This methyl-cation transfer reaction is known to occur with the melting of solid betaine (m.p. 310°C),[23] but the barrier for this isomerization in the gas phase is expected to be significantly higher.

A question may be raised regarding the gas phase structures of the protonated "betaine"-base adducts and whether the measured proton affinity is truly that of betaine, and not of the methyl ester or their mixture. Our experimental results indicate that the adducts containing betaine are the predominant forms generated with the method described. The proton affinity of the methyl ester has been measured by Cooks and co-workers as 227.2 kcal/mol.[24] This is significantly lower than that of the reference bases used in our experiments. With differences this large (9–21 kcal/mol), CID of the adducts containing the ester isomers will yield the protonated bases as the only products. No detectable amount of ions with the *m/z* corresponding to the protonated ester will be produced. It is also unlikely that the adduct populations were mixtures with significant

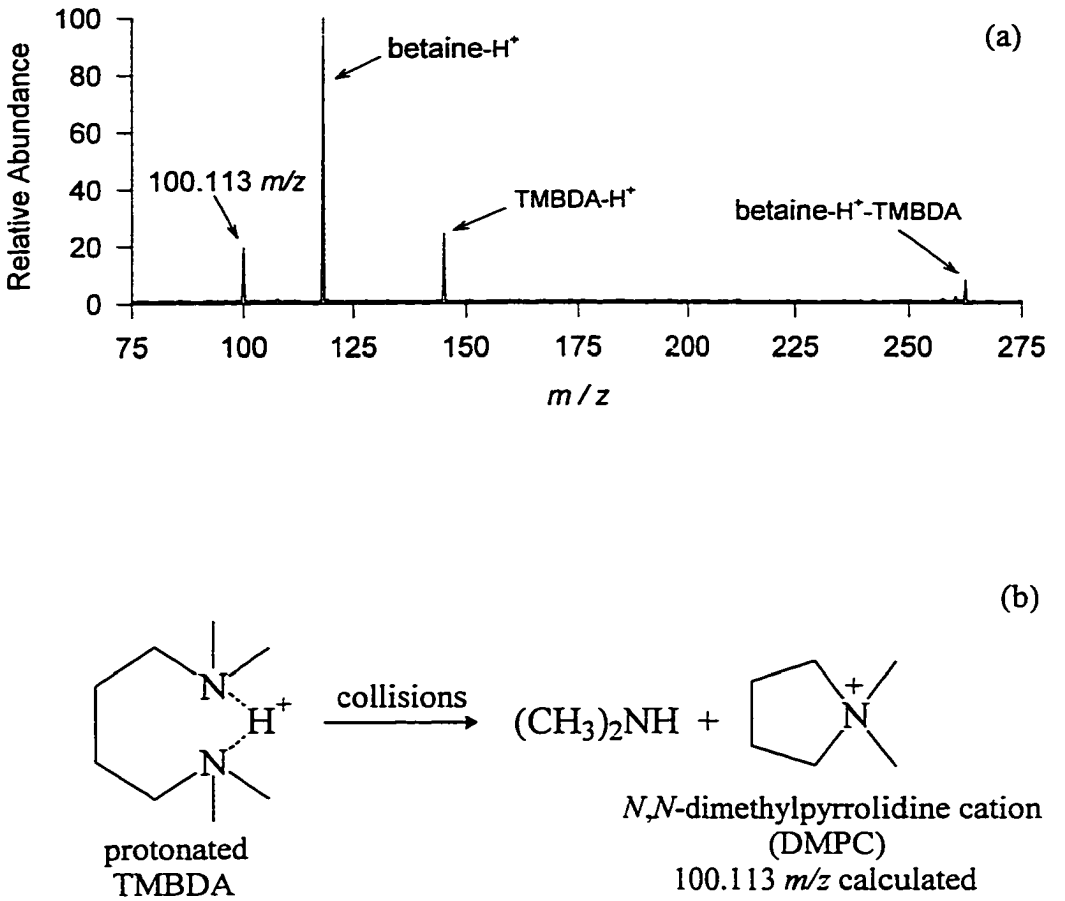

Figure 1.5: (a) Spectrum of protonated betaine-TMBDA adduct after CID at 1.1 eV average collision energy in the center-of-mass frame. (b) A possible reaction scheme for the secondary fragmentation of protonated TMBDA.

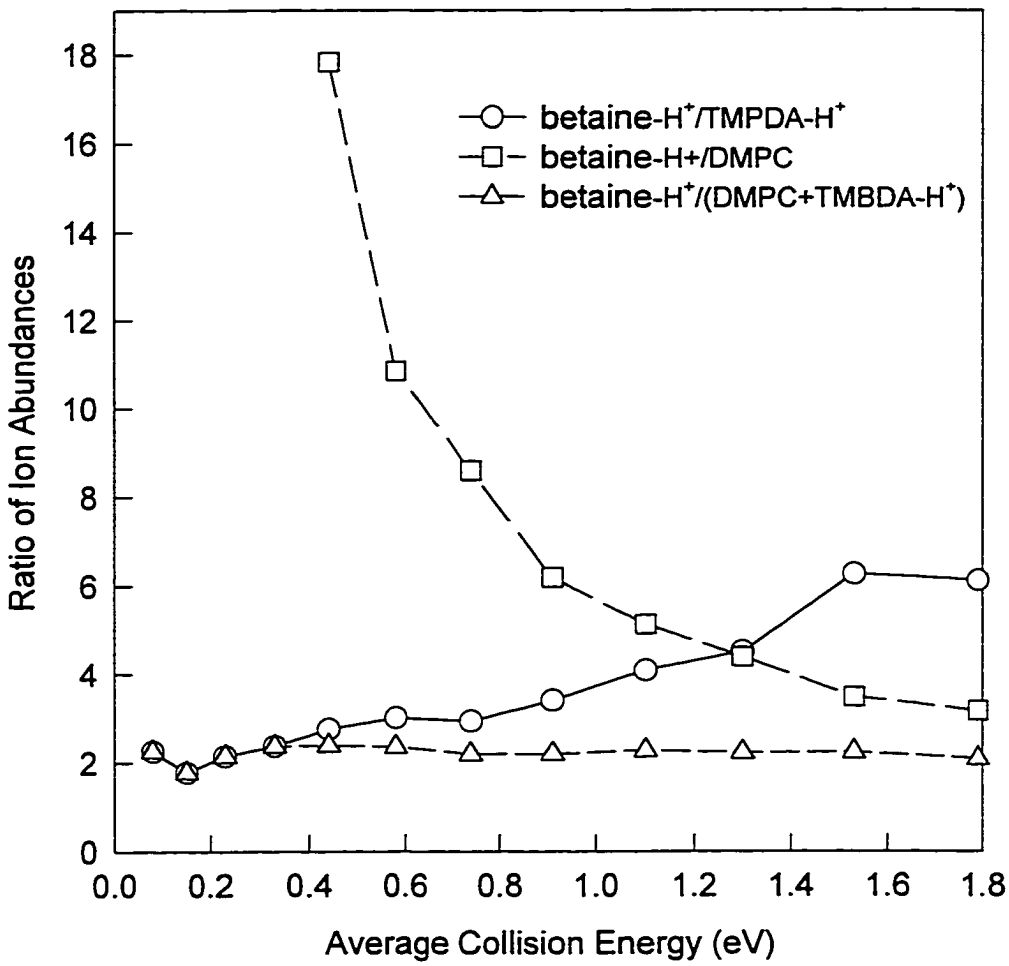

Figure 1.6: The ratios of ion abundances resulting from CID of protonated betaine-TMBDA adduct plotted against the average collision energy in the center-of-mass frame. DMPC refers to the ion at 100.113 *m/z* (figure 1.5a), which is tentatively assigned as *N,N*-dimethylpyrrolidine cation (figure 1.5b).

amounts of the methyl ester isomer. This is experimentally supported by the CID result of the betaine/TBA (E_{PA} = 236.0 kcal/mol) system, which indicates that at least 97% of the adducts are composed of the zwitterion form.

The difference of 103 ± 2 kcal/mol in the proton affinities of *t*-butylacetate anion and betaine indicates that a nearby positive charge can give rise to an enormous increase in the acidity of a carboxylic acid group. The contribution of electrostatic stabilization to this difference can be roughly estimated from the energy of interaction between two point charges, given by Coulomb's law in the form of eqn. 30 (cgs units):

$$E = \frac{q_1 q_2}{r D} \qquad [1.29]$$

in which q_1 and q_2 are the charges of the two groups, r is the distance between them, and D is the dielectric constant of the medium (solvent). D is equal to 1.0 in vacuum, 1.9 in hexane, and 79 in water.[25] Shielding by a methylene group between two charges in the gas phase is negligible,[26] and D is expected be very close to 1.0 in isolated betaine. Substituting 3.3 Å for r, the magnitude of dipolar stabilization in betaine calculated using eqn. 29 is 101 kcal/mol. Such a close agreement between a simple Coulomb's law calculation and an experimental measurement of electrostatic effect on the chemistry of a functional group was also observed by Williams *et al.*,[26] in their investigation of the influence of Coulomb repulsion on the gas phase basicity of protonated diaminoalkanes. More experimental studies on this subject are certainly required. But for reactions involving charged intermediates, these results imply that the thermochemical effects of

distal charge centers on other functional groups may be adequately described as purely electrostatic in nature.

1.5 Conclusions

The RRK rationalization of the kinetic method introduced by Campbell *et al.*[8] has been expanded and generalized using RRKM unimolecular reaction theory. Unlike the often invoked analysis using transition state theory, these derivations do not assume a Boltzmann distribution of internal energies in the reacting ions, reinforcing the validity of the kinetic method. The RRKM rationalization provides a general expression relating the ion product population ratio to the proton affinity difference. It is independent of the modes used to model the internal degrees of freedom in the reacting ion and the transition state, but reduces to the RRK expression when the appropriate physical model is applied.

Experimental application of the kinetic method has been demonstrated in the determination of the gas phase proton affinity of betaine. The measured value is 242 ± 1 kcal/mol, or 103 kcal/mol less than the proton affinity of its isoelectronic analog, *t*-butylacetate anion. Most of this difference, ~101 kcal/mol, is attributed to the dipolar stabilization of the carboxylate anion in betaine and represents the increase in the acidity of a carboxylic acid group that would arise from the presence of an isolated positive charge 3.3 Å away. This is one of the first reported experimental measurements of such electrostatic effect on the chemical properties of a function group.[27]

1.6 References and Notes

(1) Stryer, L. *Biochemistry*, 4th ed.; Freeman: New York, 1995; Chapter 9.

(2) The lowest-energy structures were calculated semi-empirically (PM3 method) using Hyperchem™ Computational Chemistry Software Package, Version 4.0, Hypercube Inc., 1994.

(3) (a) Aue, D. H.; Bowers, M. T. *Gas Phase Ion Chemistry*; Academic Press: New York, 1979; Vol. 2. (b) Henderson, W. G.; Taagepera, M.; Holtz, D.; McIver, R. T., Jr.; Beauchamp, J. L.; Taft, R. W. *J. Am. Chem. Soc.* **1972**, *94*, 4728.

(4) Caldwell, G.; Renneboog, R.; Kebarle, P. *Can. J. Chem.* **1989**, *67*, 611.

(5) (a) Cooks, R. G.; Kruger, T. L. *J. Am. Chem. Soc.* **1977**, *99*, 1279. (b) Majumdar, T. K.; Clairet, F.; Tabet, J.-C.; Cooks, R. G. *J. Am. Chem. Soc.* **1992**, *114*, 2897. (c) Cooks, R. G.; Patrick, J. S.; Kotiaho, T.; McLuckey, S. A. *Mass Spectr.* **1994**, *13*, 287.

(6) (a) Chen, L.-Z.; Miller, J. M. *Org. Mass Spectrom.* **1992**, *27*, 883. (b) Makelnia, S.; Brodbelt, J. *J. Am. Chem. Soc.* **1992**, *114*, 4295. (c) Bojesen, G.; Breindahl, T.; Andersen, U. N. *Org. Mass Spectrom.* **1993**, *28*, 1448. (d) Burinsky, D.; Fukuda, E. K.; Campana, J. E. *J. Am. Chem. Soc.* **1984**, *106*, 2770.

(7) Cheng, X.; Wu, Z.; Fenselau, C. *J. Am. Chem. Soc.* **1993**, *115*, 4844.

(8) Campbell, S.; Marzluff, E. M.; Rodgers, M. T.; Beauchamp, J. L.; Rempe, M. E.; Schwinck, K. F.; Lichtenberger, D. L. *J. Am. Chem. Soc.* **1994**, *116*, 5257.

(9) Greco, F.; Liguori, A.; Sindona, G.; Uccella, N. *J. Am. Chem. Soc.* **1990**, *112*, 9092.

(10) Bojesen, G.; Breindahl, T. *J. Chem. Soc. Perkin Trans. 2* **1994**, *5*, 1029.

(11) Rodgers, M. T.; Campbell, S.; Marzluff, E. M.; Beauchamp, J. L. *Int. J. Mass Spectrom. Ion Processes* **1994**, *137*, 121.

(12) Marzluff, E. M.; Campbell, S.; Rodgers, M. T.; Beauchamp, J. L. *J. Am. Chem. Soc.* **1994**, *116*, 7787.

(13) Schulz, G. J.; Phelps, A. V. *Rev. Sci. Instrum.* **1957**, *28*, 1051.

(14) (a) Decouzon, M.; Gal, J.-F.; Maria, P.-C.; Raczynska, E. D. *J. Org. Chem.* **1991**, *56*, 3669. (b) Raczynska, E. D.; Maria, P.-C.; Gal, J.-F.; Decouzon, M. *J. Org. Chem.* **1992**, *57*, 5730. A $T\Delta S$ value of 7.8 kcal/mol was used to calculate the proton affinities from the gas phase basicities furnished.[15]

(15) Decouzon, M.; Gal, J.-F.; Maria, P.-C.; Raczynska, E. D. *Rapid Commun. Mass Spectrom.* **1993**, *7*, 599.

(16) Gauthier, J. W.; Trautman, T. R.; Jacobson, D. B. *Anal. Chim. Acta* **1991**, *246*, 211.

(17) Robinson, R. J.; Holbrook, K. A. *Unimolecular Reactions*; Wiley: London, 1973; Chapters 3-5.

(18) Meot-Ner, M. In *Molecular Structure and Energetics*; Liebman, J. F., Greenberg, A., Eds.; VCH: New York, 1987; Vol. 4; Chapter 3.

(19) Forst, W. *Theory of Unimolecular Reactions*; Academic Press: New York, 1973; in particular pp 93-95.

(20) Edwards, J. *A Treatise on the Integral Calculus*; Chelsea Publishing: New York, 1954; Vol. II; Chapter XXV.

(21) Yu, D.; Armstrong, D. A.; Rauk, A. *Can. J. Chem.* **1992**, *70*, 1762.

(22) Price, W. D.; Jockusch, R. A.; Williams, E. R. *J. Am. Chem. Soc.* **1997**, *119*, 11988.

(23) Beilstein, F. K. In *Beilsteins Handbuch der organischen Chemie*; Boit, H.-G., Ed.; Springer-Verlag: Berlin, 1963; **4**-346.

(24) Patrick, J. S.; Yang, S. S.; Cooks, R. G. *J. Am. Chem. Soc.* **1996**, *118*, 231. A $T\Delta S$ value of 7.8 kcal/mol was used to calculate the proton affinity from the gas phase basicity furnished (see Reference 14).

(25) In *Handbook of Chemistry and Physics*, 74th ed.; Lide, D. R, Ed.; CRC Press: Boca Raton, 1993-1994.

(26) Gross, D. S.; Rodriguez-Cruz, S. E.; Bock, S.; Williams, E. R. *J. Phys. Chem.* **1995**, *99*, 4034.

(27) The gas phase basicity(GB) of betaine has been determined by Cooks and co-workers with a quadrupole mass spectrometer using the kinetic method. Their result (GB = 232.9 ± 0.8 kcal/mol) is consistent with our proton affinity measurement. Patrick, J. S.; Yang, S. S.; Cooks, R. G. *J. Am. Chem. Soc.* **1996**, *118*, 231.

Chapter 2: High Resolution Spectroscopy of Trapped Ions: Concept and Design

2.1 Introduction

Chemistry of small and medium-sized molecular ions in the gas phase has been extensively studied during the last four decades. Much of the progress has been made possible by the advent of experimental methods such as crossed beams, ion drift tubes, and mass spectrometry techniques,[1] which all take advantage of the ease of manipulating charged particles. Quantitative insights into the kinetics and thermochemistry of ion-molecule reactions and unimolecular processes in ions have been obtained that rival, if not surpass, the knowledge of such chemical properties in neutral gas molecules.

Physical properties of gas phase ions, however, are far less well known. Their structures, electric and magnetic multipole moments, low-frequency internal motions, and other molecular parameters which can reveal the electronic wavefunction remain largely uninvestigated experimentally. This is in sharp contrast to the study of neutral systems, where the high resolution and accuracy afforded by spectroscopy in the radio and microwave frequencies have provided a wealth of knowledge on these properties. Study of ions at these frequencies has been limited to lower resolutions and to a small number of species which can be generated favorably in continuous discharge ion sources.[2]

The lack of precise and general spectroscopic methods has forced chemists to attempt to extract physical properties of gas phase ions from their chemical properties, often augmented with computational work of varied sophistication. An example of this is to infer the structure of an ionic cluster from its reactivity with neutral gases. A need for a high resolution spectroscopic technique for ions is also apparent in chemical analysis. In a complex mixture of many neutral and ionic species, for example in interstellar gases and in combustion of fuels, often only the radio and microwave regions have the necessary resolution and accuracy to identify the components from its absorption spectra. However, since spectra of most molecular ions in these frequencies are not known, only the neutral species can be recognized.

The difficulty in spectroscopy of gas phase ions arises from the same feature that makes the study of their chemical properties facile: Their charged state leads to electrostatic repulsion, resulting in low sample density. The small number of photons being absorbed or emitted by the system under investigation makes detection difficult, especially if the radiation is of low energy. A solution to this type of problem was demonstrated by the molecular beam magnetic resonance experiments of Rabi and co-workers. Their scheme, in which the resonance absorption of radiation is detected by its effect on the absorbing molecule rather than on the radiation, has since been utilized in other experiments to investigate neutral systems.[3]

Pizarro and Weitekamp[4] have proposed an experimental technique employing such a detection method for obtaining high-resolution spectroscopy of molecular ions, termed internally resonant ion trapping excitation (IRITE). Although developed for studying magnetic resonances, the authors have also suggested adaptation of the

technique for electric dipole transitions in the radio and microwave frequencies. The present proposal builds upon this suggestion and describes in detail an experiment to observe r.f. resonances using IRITE. This novel technique, readily adaptable to microwave frequencies, not only promises spectroscopy of a wide variety of molecular and cluster ions, but with the spectral resolution currently unattainable even for neutral systems.

2.2 Internally Resonant Ion Trapping Excitation

The theoretical background of the proposed experiment is briefly discussed in this section. A superposition of two energy levels created by a resonant electric field has a macroscopic dipole moment which oscillates in the laboratory frame. If the resonant field is spatially inhomogeneous, then the particle with the dipole moment experiences an accelerating force from the interaction between the moment and gradient of the field: The particle is spatially displaced. This phenomenon has been observed in neutral atoms with high-powered lasers and is called the radiative, or the gradient, dipole force.[5]

In IRITE, this on-resonance spatial displacement is detected as a change in the oscillatory motions of ions trapped in an ion cyclotron resonance (ICR), or Penning, cell. The gradient field is applied as time-varying potential differences among electrodes of the cell (for r.f. experiments) or by using the cell as a microwave cavity (for microwave experiments). Although originally developed for the cyclotron motion in a magnetic field, the theory of IRITE can be adapted to any harmonic oscillation of a trapped particle,

including the magnetron and the axial motion in an ICR cell. In the particular experiment proposed here, r.f. IRITE will be detected as a change in the energy of axial oscillation.

The gradient field to be used in the proposed experiment is of the form

$$\bar{E}(\bar{r},\, t) = G(x\,\hat{\mathrm{i}} + y\,\hat{\mathrm{j}} - 2z\,\hat{\mathrm{k}})\left[\cos(\omega_o + \omega_z)t + \cos(\omega_o - \omega_z)t\right], \qquad [2.1]$$

where G is the magnitude of gradient, ω_o the (angular) frequency of the internal resonance, and ω_z the axial trapping frequency. Here the z-axis is defined to be along the magnetic field line. Any spatially inhomogeneous field can couple internal states with the external translational motion. Since the electrodes making up an ICR cell can be divided into any number of pieces,[6] a wide variety of r.f. field configurations are possible. The quadrupolar configuration of eqn. [2.1] has the advantage of being simple to implement (with a.c. potential differences between the ring and the endcap electrodes of an ordinary ICR cell) and having the z-component required for the parallel transitions ($\Delta M_J = 0$) we wish to examine in this particular experiment. [The same field applied at $\cos(\omega_o + \omega_+)t$, where ω_+ is the cyclotron frequency, for example, can be used to excite the cyclotron motion for perpendicular transitions.] Furthermore, the ponderomotive potential resulting from this r.f. field can be easily neutralized by lowering the d.c. trapping voltage.[7]

With the gradient field applied at the sum and the difference of the internal and axial frequencies, it has the effect of driving the axial motion in proportion to the transition dipole moment created by the field. A rotating frame analysis predicts a change in the oscillation energy of

$$\Delta E_z = \pm \frac{(\mu G t)^2}{2m}, \qquad [2.2]$$

where μ is the magnitude of the dipole moment, t the length of time IRITE is applied, and m the mass of the ion (see Appendix A). The ± sign indicates that the ion will be either accelerated or decelerated by IRITE, depending on which of the two eigenstates of the transition dipole the ion was in before the application of IRITE. If the initial axial energy is small compared to ΔE_z, then ions in both states are accelerated, but with a 180° difference in the axial phase. Substituting in the experimental parameters,

$$\Delta E_z = \pm \frac{0.07}{m} \left(\frac{\mu V_{RF} t}{r_o^2} \right)^2 ; \qquad [2.3]$$

V_{RF} is the peak voltage of the applied r.f., and r_o is the radius of the cylindrical cell to be used in the experiment. With m = 36 amu, μ = 1 Debye, V_{RF} = 200 $V_{0\text{-}p}$, t = 1 sec, and r_o = 3 mm, the anticipated change in the energy of oscillation is ± 40 meV.

Useful spectroscopy, however, cannot be performed simply by observing the frequency-dependence of this energy change. The large magnitude of electrical field needed to create the strong gradient will completely mix the internal states, resulting in spectra that are significantly power-broadened and difficult to interpret. For the r.f. experiment proposed here, the Rabi frequency associated with the gradient field can be as

large as, or even larger than, the internal transition frequencies, depending on the position of ion in the cell.

The proposed experiment overcomes this problem by taking advantage of the near-collisionless conditions in an ICR trap and obtaining the spectra in the time domain. This is facilitated by applying a homogeneous r.f. field in addition to the gradient field, to make IRITE uniformly effective across some broad spectral region. This field, referred here as the dipole-locking field, allows transition dipoles with resonance frequencies across a wide spectrum to remain in phase with the IRITE force, allowing all of the transitions to be excited nearly equally. Addition of a dipole-locking field of magnitude ε modifies eqn. [2.1] to give the new gradient field,

$$\bar{E}(\bar{r},\, t) = G\left(x\,\hat{\mathrm{i}} + y\,\hat{\mathrm{j}} - 2z\,\hat{\mathrm{k}}\right)\left[\cos\left(\omega+\omega_z\right)t + \cos\left(\omega-\omega_z\right)t\right] + \varepsilon\,\hat{\mathrm{k}}\cos\omega t, \qquad [2.4]$$

where ω is some convenient frequency in the spectral region of interest.

Taking into account the effect of the dipole-locking field, eqn. [2.2] now becomes

$$\Delta E_z = \pm\frac{\left(\mu G t\right)^2}{2m}\cdot\left(\frac{\omega_1}{\sqrt{\omega_1^2+\Delta\omega^2}}\right), \qquad [2.5]$$

where ω_1 is the Rabi frequency associated with the dipole-locking field, $\omega_1 = \mu\cdot\varepsilon/\hbar$, and $\Delta\omega$ is the detuning frequency, $\Delta\omega = \omega - \omega_0$. The factor in the parentheses of eqn. [2.5] gives the effectiveness of IRITE off resonance. For example,

assuming $\mu = 1$ Debye, a dipole-locking field strength $\varepsilon = 10$ V/cm will provide an IRITE effectiveness of greater than 90% over a 5 MHz bandwidth. A field strength of $\varepsilon = 1$ kV/cm will produce an effectiveness of greater than 90% over a 500 MHz bandwidth.

The time-domain data is obtained in a manner analogous to Ramsey's molecular beam method with separated oscillating fields,[3] except that in IRITE the fields are separated in time rather than in space. In this scheme, the time in which the gradient field is applied is divided into two halves, and a period of field-free evolution of the internal states is introduced in-between. The effects of the two periods of gradient field either add or subtract from each other, depending on whether the internal state of the ion has remained the same or changed to the other eigenstate of the transition dipole during the free evolution period. If the state had remained the same, then the net result is identical to that with no free evolution period in-between. If it did switch, then the effects of the two periods cancel out each other and there is no net energy change (see Appendix B).

The probability of an ion's internal state remaining the same during the free evolution period t_1 is[3]

$$P = \frac{1}{2}\left(1 + \cos \Delta\omega \, t_1\right) . \qquad [2.6]$$

The spectroscopic information is obtained by varying the length of t_1. For example, with a detection scheme that only detects ions in which the effects of the two IRITE periods add, the signal amplitude obtained at various t_1 will modulate at $\Delta\omega$. If the bandwidth of the experiment covers several transitions of different ω_o's, then the signal will be a sum

of such modulations. Fourier transform of this time-domain signal provides the desired spectrum unperturbed by the gradient field.

2.3 Experimental Considerations

Purpose of the planned experiment is to demonstrate the feasibility of IRITE by obtaining high resolution r.f. spectra of $H^{35}Cl^+$ and $H^{37}Cl^+$. It is designed to be performed on a commercial FT-ICR mass spectrometer with modest modifications.

2.3.a Overview of the Experiment. The experiment is carried out using a dual-cell configuration: one to perform ICR mass spectrometry (MS cell) and the other for IRITE (IRITE cell). A population of HCl^+ ions is generated by electron impact in MS cell, and their internal and axial energies are collisionally cooled to the temperature of the cell (77 K). A small fraction of the ions (~ 100 ions) is then transferred to IRITE cell, where the gradient field is applied as a.c. voltages on the endcaps for two periods of 0.5 sec with a delay of t_1 in-between. Ions whose axial energy is excited during both periods of IRITE are released from the cell by lowering the trapping voltage on one of the endcaps and counted by a multi-channel plate detector. Ions which are not excited, or not excited enough, remain in the cell, allowing more than one time-domain data point to be taken from a single population if desired. A new "sample" of the cooled ions is then transferred from MS cell to IRITE cell to repeat the process for another t_1 data point.

2.3.b ICR Spectrometer Requirements. There must be negligible ion-molecule interaction during the one second of IRITE to avoid collision-induced relaxation of

internal states. Examination of the small amount of literature available on the low-energy relaxation rates for gas phase ions[8] suggests that a pressure in the low 10^{-10} Torr range is necessary. Fortunately, this is the typical operating pressure in many high-performance ICR instruments available commercially.

Because of the dual-cell configuration and the detection scheme to be used in the experiment, a solenoid-type magnet is required. Since it is the axial oscillation of ions that is being excited, and not the cyclotron motion, strength and field homogeneity of the magnetic field do not play critical roles in this experiment. Higher fields are desirable, however, for better trapping of ions ($\geq$ 2 tesla).

An internal ion source is preferred to avoid the wide axial energy distribution of a typical external source. This requires a pulsed valve to inject HCl gas into MS cell equipped with an electron gun. A second valve for a non-reactive gas like N_2 is needed to collisionally cool the generated ions. Resonant azimuthal quadrupole excitation[9] will be applied during the collisions to confine and mass-select HCl^+. Spontaneous emission following the collisions will augment the cooling of the internal degrees of freedom, with the average lifetime of first excited rotational level calculated to be about 30 seconds assuming a transition moment of 1 Debye.

2.3.c Modifications of ICR Instrument. An open-ended cylindrical cell will be added and used as IRITE cell (Fig. 2.1). The ability to tune and compensate for the anharmonicity in the cell's trapping potential is required, since the amplitude dependence of axial frequency effects the maximum steady-state energy that can be obtained by the IRITE driving force.[10] Although sweeping the frequency of the gradient field during excitation (i.e., chirping) can overcome this problem, the anharmonicity must still be

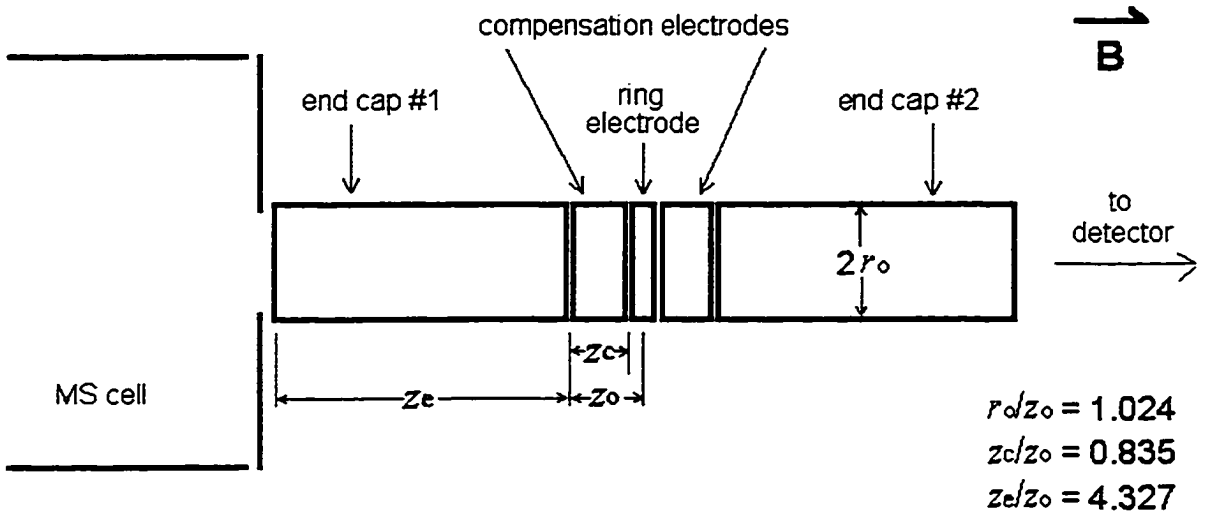

Figure 2.1: The orthogonalized, open-ended cylindrical trap to be used in the experiment as IRITE cell ($r_0 = 3$ mm). The design is from Gabrielse *et al.*[11]

minimized to keep the bandwidth of the sweep, and thus the necessary r.f. power, small. For example, a 40 meV axial energy gain corresponds to a 0.3 mm increase in the amplitude from the center of cell with the trapping voltage V_T = 10 V ($\omega_z/2\pi$ = 237.8 kHz). In a cell with the octopole expansion coefficient $|C_4| = 1 \times 10^{-2}$, this will result in a ~ 20 Hz shift in axial frequency. For $|C_4| = 1 \times 10^{-3}$, the shift will be ~ 2 Hz. Values of $|C_4|$ less than 10^{-4} have been attained for cells of same design.[12]

The experiment is simplified by cooling the axial motion and minimizing the spatial distribution of the ion cloud before application of IRITE. At 77 K, k_BT is 6.6 meV. Less than one-in-1000 ions in this thermal cloud will have axial energy of 40 meV or greater. Such a small distribution in energy effectively increases the signal-to-noise ratio of the experiment.

The cells can be cooled by taking advantage of the cryogenic pumps which many commercial ICR instruments are equipped with. A heat shield, connected via a cold finger to the pump, can be built around the cells. Since these pumps typically operate at near 10 K, a relatively simple shield will be capable of cooling the cells to ~ 77 K (Fig. 2.2). If vibration from the pump is not a problem, the cell electrodes and wires can be placed in thermal contact with the heat shield through ceramics for better cooling. R.f. heating of IRITE cell should not be significant, due to the modest capacitance expected for the circuit containing the cell and the small resistivities of materials at the low temperature. Taking into account the skin effect at 100 MHz, resistance of the cell (Ag-plated) at 77 K is estimated to be $\sim 2 \times 10^{-3}\ \Omega$.

The ions excited by IRITE can be selectively detected by slowly lowering the trapping voltage on the endcap (#2 in Fig. 2.1) until they are ejected from the cell. However, with the excitation taking place at V_T = 10 V, the trapping voltage must be lowered to less than 1 mV for the ejection to occur due to adiabatic cooling[13] of the axial oscillation. Patch effect and static charge build-ups on the cell electrodes make such a small potential difficult to obtain reproducibly. A more practical way is to ground the endcap and instead apply the trapping voltage on the adjacent compensation electrode; in effect shortening the cell. Ions with 40 meV axial energy will eject with $V_T \sim 20$ mV on the compensation electrode.

A MCP-based detection system will be utilized in this experiment. It provides the high sensitivity required without the specialized electronics necessary for non-destructive detection methods,[12,14] which may be reserved for future work. As demonstrated by the time-of-flight ICR experiments (ISOLTRAP),[15] the ions excited out of the cell will be

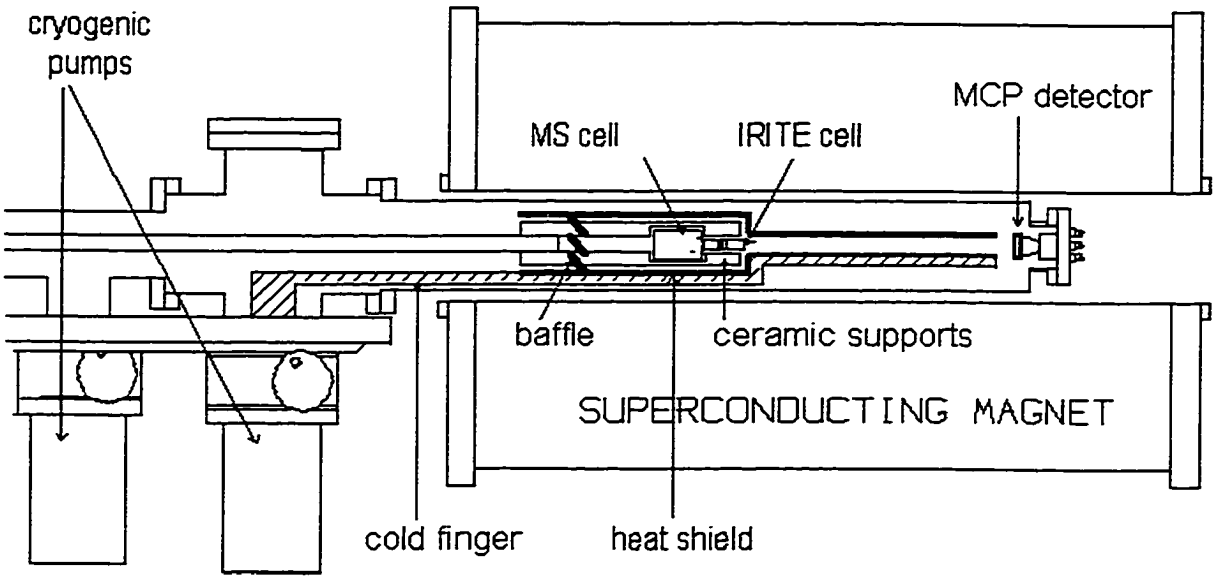

Figure 2.2: Schematic of the heat shield and the detector system. The figure depicts a section of a typical high-field FT-ICR mass spectrometer. [This setup is also useful for detecting IRITE of the cyclotron motion by measuring the ions' time of flight.]

effectively guided by the magnetic field to the detector positioned at the end of the vacuum chamber.

2.3.d Target Spectra. The internal resonances of interest are the transitions between the two members of Λ-type doublets in the lowest rotational levels of $H^{35}Cl^+$ and $H^{37}Cl^+$: $J = 3/2$ and 5/2 of the spin-orbit substate $\Omega = 3/2$, $\upsilon = 0$. These transitions are expected to occur near 90 and 340 MHz,[16] respectively, with $\Delta M_J = 0$. HCl^+ is a good $^2\Pi$ case (*a*) system in the lower rotational levels, and the field strength of an ICR magnet (1 ~ 7 Tesla) is not large enough to produce a full Paschen-Back effect, since the spin-orbit coupling constant is $-634\ cm^{-1}$.

The Λ-doublet transition for each rotational level will have Zeeman splitting as well as hyperfine structure. Since the Zeeman energies are much larger than hyperfine

energies, each M_J component will be examined in a separate experiment to keep the bandwidth of the experiment small and the electronic circuitry of the apparatus simple. For example, the four Zeeman components of the $J = 3/2$ level of $H^{35}Cl^+$ will be spread out over 9 MHz at 2 Tesla, while the hyperfine splittings of each component should be covered by a 100 kHz bandwidth.[17] A more quantitative prediction of the spectra is not possible with the current knowledge of molecular constants for HCl^+.

2.3.e Data Acquisition. Time line for the proposed experiment is shown in Fig. 2.3. All d.c. trapping voltage changes are to be done slow enough to effect the ion cloud adiabatically. The number of ions transferred from MS cell to IRITE cell will be kept small (~ 100) to minimize undesirable effects of ion-ion interaction during IRITE.

A potential source of noise in the time-domain signal is the fluctuation in the number of ions generated and transferred to IRITE cell. This uncertainty is avoided by counting the total number of ions in the cell (see Fig. 2.3) and normalizing the signal count obtained from that population. This leaves the counting statistics from quantum uncertainty as the principal noise source.

An estimation of the signal counts can be made assuming a Boltzmann distribution of internal states at 77 K. For the $J = 3/2$ level of $H^{35}Cl^+$, 53% of the ion population will be distributed approximately equally among its four Zeeman components. Thus, in an experiment in which the spectral bandwidth covers the hyperfine splittings of one component, at most ~ 13% of the population can be excited (i.e., axial energy increases during both IRITE periods). The actual percentage of ions excited is determined by the length of free evolution period t_1 and eqn. [2.6]. If it is assumed that

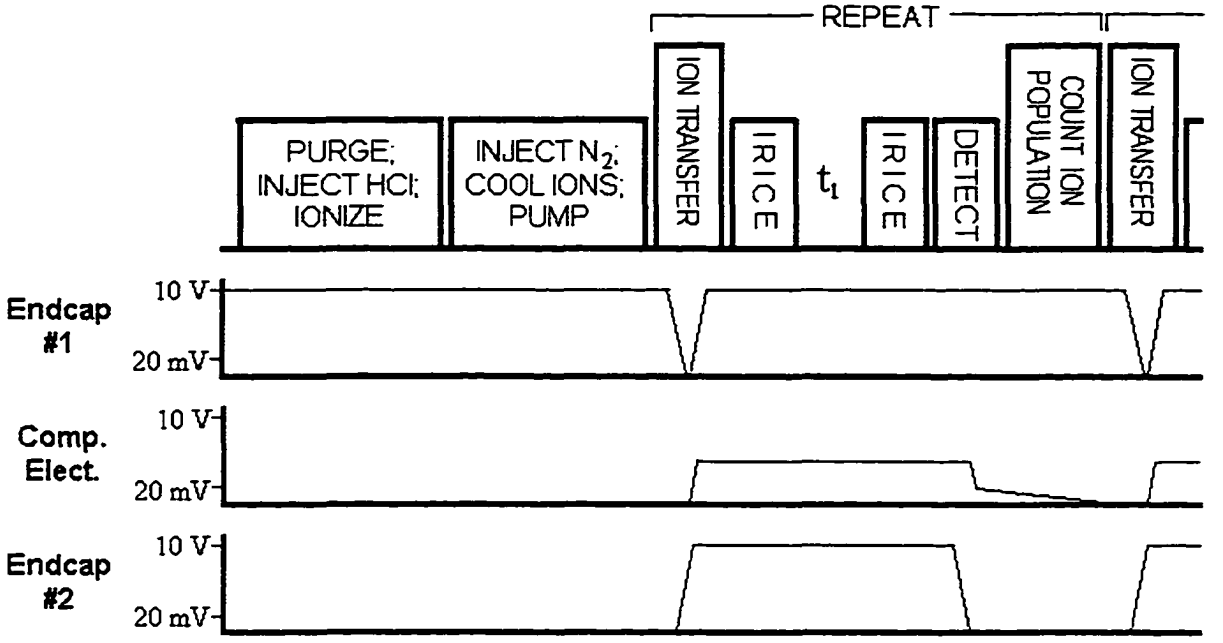

Figure 2.3: Time line for the proposed experiment. Plot labeled "Endcap #1" indicates the d.c. voltage on the endcap of IRITE cell adjacent to MS cell (see Fig. 2.1). "Comp. Elect." indicates the d.c. voltage on the compensation electrodes. "Endcap #2" indicates the voltage on the endcap closest to the detector.

only 1/3 of these ions are actually counted by the detector (due to ion loss during flight, ~50% efficiency of a typical MCP detector, etc.), then the maximum signal count is a little more than 4% of the ions in the cell per data point. Assuming 100 ions in the cell, this corresponds to 4 counts per point. A similar signal count can be expected for the J = 5/2 level, which has 32% of the population divided among six Zeeman components.

The lengths of free evolution periods t_1 will be chosen so that they are equal to integral multiples of the period of axial oscillation (4.2 μsec under the proposed conditions). Otherwise, the magnitude of driving force during the second IRITE period will decrease by a factor of $\cos[\Delta\phi]$, where $\Delta\phi$ is the difference between the axial phase at

the end of the first period and that at the beginning of the second. [Alternatively, the phase of the second IRITE period can be changed relative to that of the first period to take into account the axial motion during t_1. The change in the transition probability (eqn. [2.6]) resulting from such a phase shift[3] can be rectified by scaling the signal count.] A time-domain data acquisition of 1024 points at $\Delta t_1 = 4.2$ μsec intervals gives a frequency-domain spacing of 230 Hz per point and a bandwidth of 120 kHz. If it takes 60 seconds to generate and cool the ions, and up to 100 "samples" can be transferred to IRITE cell from each ion generation, then each scan takes ~ 1600 seconds. About 46 hours of data acquisition time is needed to average 100 scans. The anticipated time-domain signal-to-noise ratio for the experiment is roughly the square root of the total number of counts possible, or $\sqrt{400}$ in this example.

2.4 Final Comments

An ICR trap provides chemists with a unsurpassed ability to isolate and manipulate charged systems, and the novel technique introduced here promises high resolution spectroscopy of ions in such a unique environment. The experiment presented in this proposal is primarily intended to prove the concept of IRITE and designed to be carried out on an existing instrument with minimal modifications. But it can be readily combined with methods and technologies already in use in ICR mass spectrometry to bring forth the full potential of the technique. A non-destructive detection scheme with single-ion sensitivity, adapted from the high-precision mass measurement

experiments,[12,14] enables a spectrum to be obtained from a single ion population, negating the need for repeated ion generations and the dual-cell configuration. The practically indefinite containment time of the trap and its ability to operate in cryogenic temperatures (~ 4 K) allows cooling of the internal degrees of freedom, making studies of large and complex systems possible. And since the trap is compatible with most types of ion sources, including those useful for generating highly reactive species and weakly bound complexes, IRITE is a general method applicable to a wide variety of chemically interesting systems.

Impact of this new technique will extend beyond that of allowing spectroscopy of previously inaccessible systems. As demonstrated in the high-precision mass measurement and "geonium" experiments,[18] an ICR trap provides a setting in which the external influences on the system of investigation can be controlled to very high precision. This, along with the time-domain data acquisition, will enable chemists to obtain spectra with the accuracy and resolution currently not possible even for neutral molecules. The experiment described in this proposal, although not intended to achieve the ultimate precision of IRITE, will surpass the molecular beam electric resonance experiments[19] in resolution. By making available for study phenomena previously unobservable, this new technique will provide theorists and computational chemists with new questions and challenges for many years to come.

2.5 References

(1) *Gas Phase Ion Chemistry*, Bowers, M. T., ed.; Academic Press: New York, 1983.

(2) Woods, R. C. in *Molecular Ions: Spectroscopy, Structure, and Chemistry*, Miller, T. A. and Bondybey, V. E., ed.; North-Holland: Amsterdam, 1983.

(3) Ramsey, N. F. *Molecular Beams*; Oxford University Press: London, 1956.

(4) Pizarro, P. J.; Weitekamp, D. P. *Bulletin of Magnetic Resonance* **1992**, *14*, 220. Pizarro, P. J. Ph.D. Thesis, California Institute of Technology, Pasadena, 1993.

(5) Dalibard, J.; Cohen-Tannoudji, C. *J. Opt. Soc. Am. B* **1985**, *2*, 1707.

(6) Guan, S.; Marshall, A. G. *Int. J. Mass Spec. Ion Proc.* **1995**, *146/147*, 261. Schweikhard, L. *Int. J. Mass Spec. Ion Proc.* **1991**, *107*, 281.

(7) Gerlich, D. *Adv. Chem. Phys. Series* **1992**, Vol. LXXXII, 1.

(8) Anderson, T. G.; Gudeman, C. S.; Dixon, T.A.; Woods, R. C. *J. Chem. Phys.* **1980**, *72*, 1332. Buffa, G.; Tarrini, O.; Cazzoli, G.; Dore, L. *Phys. Rev. A* **1994**, *49*, 3557.

(9) Guan, S.; Kim, H. S.; Marshall, A. G.; Wahl, M. C.; Wood, T. D.; Xiang, X. *Chem. Rev.* **1994**, *94*, 2161.

(10) Brown, L. S.; Gabrielse, G. *Rev. Mod. Phys.* **1986**, *58*, 233.

(11) Gabrielse, G.; Haarsma, L.; Rolston, S. L. *Int. J. Mass Spec. Ion Proc.* **1989**, *88*, 319.

(12) Gabrielse, G.; Grobner, J.; Jhe, W.; Kalinowsky, H.; Phillips, D.; Quint, W. *Nucl. Phys. A* **1993**, *558*, 701c. Gabrielse, G.; Phillips, D.; Quint, W.; Kalinowsky, H.; Rouleau, G. *Phys. Rev. Lett.* **1995**, *74*, 3544.

(13) Dehmelt, H. G. *Adv. At. Mol. Phys.* **1969**, *5*, 109.

(14) Cornell, E. A.; Weisskopf, R. M.; Boyce, K. R.; Pritchard, D. E. *Phys. Rev. A* **1990**, *41*, 312.

(15) Bollen G. *et al.*, *Nucl. Instr. and Meth. A* **1996**, *368*, 657.

(16) Lubic, K. G.; Ray, D.; Hovde, D. C.; Veseth, L.; Saykally, R. J. *J. Mol. Spectrosc.* **1989**, *134*, 1.

(17) Radford, H. E. *Phys. Rev.* **1961**, *122*, 114.

(18) Werth, G. *J. Phys. G: Nucl. Part. Phys.* **1994**, *20*, 1865.

(19) Steinfeld, J. I. *Molecules and Radiation,* 2nd Ed.; The MIT Press: Cambridge, 1993.

Appendix A: Average Hamiltonian Theory Derivation of IRITE

Equation [2.2] of previous section, which describes the change in axial energy due to IRITE, is derived in this appendix. The calculation uses the quantum mechanical description of ion cyclotron resonance developed by Pizarro[1] to analyze the transverse Stern-Gerlach effect[2] on the cyclotron motion of trapped ions. This rotating frame analysis can readily be adapted and applied to any particle trapped in a harmonic potential, not just an ion in an ICR cell.

The total Hamiltonian of the system is written as a sum of the unperturbed Hamiltonian H_o, which describes the ion's oscillatory motions and the internal energy state, and the perturbative Hamiltonian H_1, which describes the interaction between the gradient field and the dipole moment of the ion. The rotating frame is defined by H_o:

$$H_o = H_r + H_z - \omega_o I_x \ . \qquad [A.1]$$

H_r is the radial energy operator corresponding to the cyclotron (+ subscript) and the magnetron (– subscript) motions:

$$H_r = \hbar\omega_+\left(a_+^\dagger a_+ + \tfrac{1}{2}\right) - \hbar\omega_-\left(a_-^\dagger a_- + \tfrac{1}{2}\right) \ , \qquad [A.2]$$

where $\omega_{\pm}$ is the (angular) oscillation frequency, and $a_{\pm}^{\dagger}$ and $a_{\pm}$ are the creation and destruction operators defined by Brown and Gabrielse,[3] whose exact forms are not relevant to present calculation. H_z is the axial energy operator:

$$H_z = \hbar\omega_z\left(a_z^{\dagger}a_z + \frac{1}{2}\right) , \qquad [A.3]$$

with $a_z^{\dagger}$ and a_z being the standard creation and destruction operators for a linear harmonic oscillator.[3] The resonance frequency of the internal transition being examined is ω_o, and I_x is the pseudo-spin ½ operator used to describe the internal energy state.[4] Note that the problem has both a real magnetic field (along the z-axis) and a fictitious magnetic field, whose direction is arbitrary as long as it is perpendicular to the z-axis (and chosen here to be the x-axis).

The perturbative Hamiltonian H_1 is

$$H_1 = \vec{\mu}\cdot\vec{\mathrm{E}} = \gamma\vec{I}\cdot\vec{\mathrm{E}} , \qquad [A.4]$$

where $\vec{\mu}$ is the transition dipole moment of interest and $\vec{\mathrm{E}}$ is the gradient field applied. Since the pseudo-spin ½ formalism is used, $\vec{\mu}$ is rewritten for convenience using

$$\gamma = \frac{2\mu}{\hbar} . \qquad [A.5]$$

Substituting the quadrupole field of eqn. [2.1] for $\bar{E}$,

$$H_1 = \gamma G \left(I_x x + I_y y - 2 I_z z \right) \left[\cos(\omega_0 + \omega_z)t + \cos(\omega_o - \omega_z)t \right] \quad . \qquad [A.6]$$

The goal of the calculation is to determine how the axial energy operator H_z evolves in time under the perturbation H_1 (in the rotating frame defined by H_o).

To transform H_1 to the rotating frame, we define the evolution operator as

$$U = \exp\left({}^{iH_o t}/_{\hbar} \right) \qquad [A.7]$$

and $\tilde{H}_1$, the rotating-frame H_1, as

$$\begin{aligned} \tilde{H}_1 &= U^{\dagger} H_1 U \\ &= \gamma G \left(\tilde{I}_x \tilde{x} + \tilde{I}_y \tilde{y} - 2 \tilde{I}_z \tilde{z} \right) \left[\cos(\omega_0 + \omega_z)t + \cos(\omega_o - \omega_z)t \right] . \end{aligned} \qquad [A.8]$$

Each rotating-frame operator in eqn. [A.8] can be found using the Baker-Haussdorf expansion:[5]

$$\exp(-iB\lambda)\,A\,\exp(iB\lambda) = A - i\lambda[B,A] + \left(\frac{i^2\lambda^2}{2!}\right)[B,[B,A]] \qquad [A.9]$$
$$- \left(\frac{i^3\lambda^3}{3!}\right)[B,[B,[B,A]]] + \ldots\ldots + \left(\frac{(-1)^n i^n \lambda^n}{n!}\right)[B,[B,\ldots[B,A]]\ldots]$$

where B is a Hermitian operator and λ is a real parameter. The resulting pseudo-spin ½ operators are

$$\tilde{I}_x = U^\dagger I_x U = I_x$$
$$\tilde{I}_y = U^\dagger I_y U = -I_z \sin\omega_o t + I_y \cos\omega_o t \qquad [A.10]$$
$$\tilde{I}_z = U^\dagger I_z U = I_z \cos\omega_o t + I_y \sin\omega_o t \ .$$

Among the spatial operators, only the z-operator effects the result of this calculation:

$$\tilde{z} = \sqrt{\frac{\hbar}{2m\omega_z}}\left[\left(a_z^\dagger + a_z\right)\cos\omega_z t - i\left(a_z^\dagger - a_z\right)\sin\omega_z t\right]. \qquad [A.11]$$

[See reference 1 for corresponding expressions for x and y.] Substituting in the individual operators into eqn. [A.8], the perturbative Hamiltonian in the rotating frame is

$$\begin{aligned}\tilde{H}_1 \;=\; & \gamma G\left(\tilde{I}_x\,\tilde{x}+\tilde{I}_y\,\tilde{y}\right)\left[\cos(\omega_0+\omega_z)t+\cos(\omega_o-\omega_z)t\right] \\ & -\gamma G\sqrt{\frac{\hbar}{2m\omega_z}}\;\Big\{\; I_z\left(a_z^{\dagger}+a_z\right)\left[\cos(\omega_o-\omega_z)t+\cos(\omega_o+\omega_z)t\right] \\ & \qquad +\; i\,I_z\left(a_z^{\dagger}-a_z\right)\left[\sin(\omega_o-\omega_z)t-\sin(\omega_o+\omega_z)t\right] \\ & \qquad +\; I_y\left(a_z^{\dagger}+a_z\right)\left[\sin(\omega_o-\omega_z)t+\sin(\omega_o+\omega_z)t\right] \\ & \qquad -\; i\,I_y\left(a_z^{\dagger}-a_z\right)\left[\cos(\omega_o-\omega_z)t-\cos(\omega_o+\omega_z)t\right]\Big\} \\ & \qquad\qquad \times\left[\cos(\omega_0+\omega_z)t+\cos(\omega_o-\omega_z)t\right].\end{aligned} \qquad \text{[A.12]}$$

Removing the explicit time dependence by averaging each term over time, the average rotating frame Hamiltonian is obtained:

$$\tilde{H}_1^{(0)} = -\gamma G\sqrt{\frac{\hbar}{2m\omega_z}}\,I_z\left(a_z^{\dagger}+a_z\right). \qquad \text{[A.13]}$$

The axial energy operator H_z also needs to be transformed to the rotating frame, but since it commutes with all of the terms in H_o,

$$\tilde{H}_z = U^{\dagger}\,H_z\,U = H_z\;. \qquad \text{[A.14]}$$

Time evolution of H_z under the perturbation of the gradient field can now be determined. Again using the Baker-Haussdorf expansion (eqn. [A.9]),

$$\begin{aligned}\widetilde{H}_z(t) &= \exp\left(i\widetilde{H}_1^{(0)}\,t/\hbar\right)\widetilde{H}_z\,\exp\left(-i\widetilde{H}_1^{(0)}\,t/\hbar\right)\\ &= \widetilde{H}_z + \frac{it}{\hbar}\left[\widetilde{H}_1^{(0)},\,\widetilde{H}_z\right] + \frac{1}{2!}\left(\frac{it}{\hbar}\right)^2\left[\widetilde{H}_1^{(0)},\left[\widetilde{H}_1^{(0)},\,\widetilde{H}_z\right]\right] \qquad \text{[A.15]}\\ &\quad + \frac{1}{3!}\left(\frac{it}{\hbar}\right)^3\left[\widetilde{H}_1^{(0)},\left[\widetilde{H}_1^{(0)},\left[\widetilde{H}_1^{(0)},\,\widetilde{H}_z\right]\right]\right] + \ldots\ldots .\end{aligned}$$

The commutators in the expansion are

$$\begin{aligned}\left[\widetilde{H}_1^{(0)},\,\widetilde{H}_z\right] &= -\hbar\omega_z\gamma G\sqrt{\frac{\hbar}{2m\omega_z}}\,I_z\left(-a_z^\dagger + a_z\right)\\ \left[\widetilde{H}_1^{(0)},\left[\widetilde{H}_1^{(0)},\,\widetilde{H}_z\right]\right] &= -\frac{(\hbar\gamma G)^2}{m}I_x^2 \qquad \text{[A.16]}\\ \left[\widetilde{H}_1^{(0)},\left[\widetilde{H}_1^{(0)},\left[\widetilde{H}_1^{(0)},\,\widetilde{H}_z\right]\right]\right] &= 0\,.\end{aligned}$$

Higher order commutators, and terms containing them, vanish, leaving

$$\widetilde{H}_z(t) = \widetilde{H}_z - i\gamma G\,t\sqrt{\frac{\hbar\omega_z}{2m}}\,I_z\left(-a_z^\dagger + a_z\right) + \frac{(\hbar\gamma G\,t)^2}{8m}\,. \qquad \text{[A.17]}$$

The first term of eqn. [A.17] corresponds to the initial axial energy. Diagonal matrix elements of the second term will be zero and not contribute to the final energy. The change in ion's axial energy will result from the last term.

With the operator now in hand, and the time dependence of the problem taken into account by the operator, the effect of IRITE on the axial energy (eqn. [2.2]) can be readily obtained from

$$E_z(t) = \left\langle \Psi(0) \right| \tilde{H}_z(t) \left| \Psi(0) \right\rangle \qquad \text{[A.18]}$$

and

$$\left| \Psi(0) \right\rangle = \left| \Psi_{ho} \right\rangle \otimes \left| \Psi_{\pm} \right\rangle . \qquad \text{[A.19]}$$

$\left| \Psi_{ho} \right\rangle$ is the harmonic oscillator wavefunction in the classical limit, which describes the axial translational motion, and $\left| \Psi_{\pm} \right\rangle$ is the pseudo-spin ½ wavefunction, which describes the relevant internal eigenstate.[1]

If there are more than one ion in the trap, however, then a more accurate description of the experiment can be given using the density matrix formalism. The expectation value of an ion cloud's axial energy can be expressed as the trace of product of the axial energy operator and the density matrix of the system:[6,7]

$$\langle E_z \rangle(t) = Tr\left[\tilde{H}_z(t)\, \rho(0) \right] . \qquad \text{[A.20]}$$

If the initial axial energy of the ions is negligible (compare to the excitation), then $\rho(0)$ can be written simply as the tensor product between the density matrix of a harmonic oscillator in thermal equilibrium and that of a unpolarized two-state system:[4]

$$\begin{aligned} \rho(0) &= \rho_{\text{H.O.}} \otimes \rho_{1/2} \\ &= Z^{-1} \exp\left(H_z / k_B T \right) \otimes \frac{1}{2} \underline{\underline{1}} \end{aligned} \qquad [A.21]$$

where Z is the partition function and $\underline{\underline{1}}$ is the 2×2 unit matrix. Substituting eqns. [A.17] and [A.21] into [A.20],

$$\begin{aligned} \langle E_z \rangle(t) &= \Delta \langle E_z \rangle(t) \\ &= \frac{(\hbar \gamma G t)^2}{8m} = \frac{(\mu G t)^2}{2m}. \end{aligned} \qquad [A.22]$$

A.1 References

(1) Pizarro, P. J., Ph.D. Thesis, California Institute of Technology, Pasadena, 1993.

(2) Bloom, M.; Erdman, K. *Can. J. Phys.* **1962**, *40*, 179. Bloom, M.; Enga, E.; Lew, H. *Can. J. Phys.* **1967**, *45*, 1481.

(3) Brown, L. S; Gabrielse, G. *Rev. Mod. Phys.* **1986**, *58*, 233.

(4) Cohen-Tannoudji, C.; Diu, B.; Laloë, F. *Quantum Mechanics*; Hermann: Paris, 1977.

(5) Sakurai, J. J. *Modern Quantum Mechanics*; Benjamin/Cummings: Menlo Park, 1985.

(6) Fano, U. *Rev. Mod. Phys.* **1957**, *29*, 74.

(7) ter Haar, D. *Rept. Progr. Phys.* **1961**, *24*, 304.

Appendix B: Derivation of Time-Domain IRITE

In the proposed IRITE experiment, the spectroscopic information is obtained in the time domain. This is accomplished by dividing the time in which the gradient field is applied into two halves and introducing a delay in between. The length of this delay, t_1, is varied for each time-domain data point. The calculation in this appendix will show that the number of ions with net increase in axial energy after the second IRITE period modulates at the detuning frequency $\Delta\omega = \omega - \omega_0$ (eqn. [2.5]) in the t_1 space.

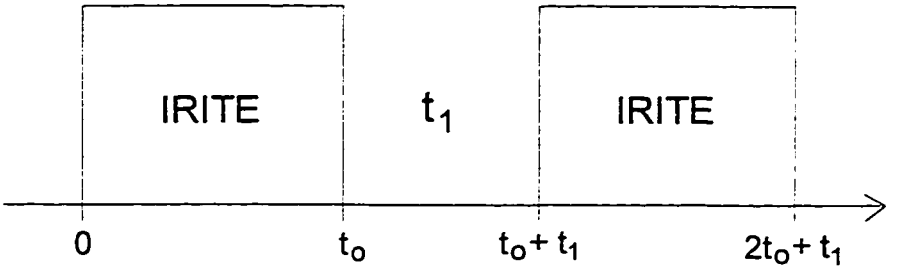

We start with an expression for the expectation value of ion cloud's axial energy in the Schrödinger picture:

$$\begin{aligned} \langle E_z \rangle(t) &= Tr\left[\tilde{H}_z\ \rho(t)\right] = Tr\left[\tilde{H}_z\ \ U^{\dagger}\rho(0)U\right] \\ &= Tr\left[\tilde{H}_z\ \ U_2^{\dagger}U_1^{\dagger}U_0^{\dagger}\rho(0)U_0\,U_1\,U_2\right], \end{aligned} \qquad \text{[B.1]}$$

where U_0 is the propagator for the first IRITE period, U_1 for the free evolution period t_1, and U_2 for the second IRITE period. The problem will be solved in the same rotating frame defined by the unperturbed Hamiltonian H_o as in Appendix A (eqn. [A.1]), so that $\tilde{H}_z = H_z$. Rewritting eqn. [B.1] in the Heisenberg picture,

$$\begin{aligned} \langle E_z \rangle(t) &= Tr\left[U_0\, U_1\, U_2 \tilde{H}_z\, U_2^{\dagger}\, U_1^{\dagger} U_0^{\dagger}\, \rho(0)\right] \\ &= Tr\left[\tilde{H}_z(t)\, \rho(0)\right]. \end{aligned} \qquad [B.2]$$

The two IRITE periods are chosen to be identical and in phase:

$$U_0 = U_2 = \exp\left(i\, \tilde{H}_1^{(0)} t_o \Big/ \hbar \right). \qquad [B.3]$$

To reduce the amount of algebra in the calculation, the time-averaged rotating frame Hamiltonian $\tilde{H}_1^{(0)}$ obtained in Appendix A (eqn. [A.13]) is used;

$$\tilde{H}_1^{(0)} = -\gamma G \sqrt{\frac{\hbar}{2m\omega_z}}\, I_z \left(a_z^{\dagger} + a_z\right). \qquad [B.4]$$

Since the derivation in Appendix A assumed a resonant gradient field, the use of $\tilde{H}_1^{(0)}$ here requires the approximation $\Delta\omega \approx 0$ for the two IRITE periods. The result is

accurate as long as ω_1, the Rabi frequency associated with the dipole-locking field (eqn. [2.5]), is much larger than $\Delta\omega$. The field-free evolution of the internal eigenstate during t_1 is expressed in the pseudo-spin ½ formalism by

$$U_1 = \exp\left(i\,\Delta\omega\,\tilde{I}_x\,t_1 \Big/ \hbar \right), \qquad \text{[B.5]}$$

where $\tilde{I}_x = I_x$ (eqn. [A.10]).

To obtain $\tilde{H}_z(t)$, we first determine the effect of the inner most propagator on the axial energy operator:

$$U_2 \tilde{H}_z U_2^\dagger = \exp\left(i\,\tilde{H}_1^{(0)} t_0 \Big/ \hbar \right) \tilde{H}_z \exp\left(-i\,\tilde{H}_1^{(0)} t_0 \Big/ \hbar \right). \qquad \text{[B.6]}$$

This is identical to eqn. [A.15] in Appendix A, except that t has been replaced by t_0. The solution is given by eqn. [A.17]:

$$U_2\,\tilde{H}_z\,U_2^\dagger = \tilde{H}_z + \frac{(\hbar\,\gamma G\,t_0)^2}{8m} - i\gamma G\,t_0\sqrt{\frac{\hbar\omega_z}{2m}}\,I_z\left(-a_z^\dagger + a_z\right). \qquad \text{[B.7]}$$

Next, propagating eqn. [B.7] under the free evolution operator $\Delta\omega\,\tilde{I}_x$,

$$U_1 U_2 \tilde{H}_z U_2^\dagger U_1^\dagger = \tilde{H}_z + \frac{(\hbar \gamma G t_0)^2}{8m} - i\gamma G t_0 \sqrt{\frac{\hbar \omega_z}{2m}} \left(-a_z^\dagger + a_z\right) U_1 I_z U_1^\dagger \ . \quad [B.8]$$

Only the I_z operator does not commute with $\tilde{I}_x$:

$$\begin{aligned} U_1 I_z U_1^\dagger = I_z &+ \frac{i\Delta\omega t_1}{\hbar}\left[\tilde{I}_x, I_z\right] + \frac{1}{2!}\left(\frac{i\Delta\omega t_1}{\hbar}\right)^2 \left[\tilde{I}_x, \left[\tilde{I}_x, I_z\right]\right] \\ &+ \frac{1}{3!}\left(\frac{i\Delta\omega t_1}{\hbar}\right)^3 \left[\tilde{I}_x, \left[\tilde{I}_x, \left[\tilde{I}_x, I_z\right]\right]\right] \\ &+ \frac{1}{4!}\left(\frac{i\Delta\omega t_1}{\hbar}\right)^4 \left[\tilde{I}_x, \left[\tilde{I}_x, \left[\tilde{I}_x, \left[\tilde{I}_x, I_z\right]\right]\right]\right] \\ &+ \frac{1}{5!}\left(\frac{i\Delta\omega t_1}{\hbar}\right)^5 \left[\tilde{I}_x, \left[\tilde{I}_x, \left[\tilde{I}_x, \left[\tilde{I}_x, \left[\tilde{I}_x, I_z\right]\right]\right]\right]\right] + \ldots\ldots \ . \end{aligned} \quad [B.9]$$

Since $\tilde{I}_x = I_x$,

$$\begin{aligned} U_1 I_z U_1^\dagger &= I_z + \Delta\omega t_1 I_y - \frac{1}{2!}(\Delta\omega t_1)^2 I_z - \frac{1}{3!}(\Delta\omega t_1)^3 I_y \\ &+ \frac{1}{4!}(\Delta\omega t_1)^4 I_z + \frac{1}{5!}(\Delta\omega t_1)^5 I_y - \ldots\ldots \end{aligned} \quad [B.10]$$

$$= I_z \cos\Delta\omega t_1 + I_y \sin\Delta\omega t_1 \ .$$

Substituting into eqn. [B.8],

$$U_1 U_2 \tilde{H}_z U_2^\dagger U_1^\dagger = \tilde{H}_z + \frac{(\hbar \gamma G t_0)^2}{8m} - i\gamma G t_0 \sqrt{\frac{\hbar \omega_z}{2m}} \left(-a_z^\dagger + a_z\right)\left(I_z \cos\Delta\omega t_1 + I_y \sin\Delta\omega t_1\right). \quad [B.11]$$

$\tilde{H}_z(t)$ can now be determined from

$$U_0 U_1 U_2 \tilde{H}_z U_2^\dagger U_1^\dagger U_0^\dagger = U_0 \tilde{H}_z U_0^\dagger + \frac{(\hbar \gamma G t_0)^2}{8m} - i\gamma G t_0 \sqrt{\frac{\hbar \omega_z}{2m}}\, U_0\left[\left(-a_z^\dagger + a_z\right)\left(I_z \cos\Delta\omega t_1 + I_y \sin\Delta\omega t_1\right)\right]U_0^\dagger. \quad [B.12]$$

The first term in eqn. [B.12] has been solved (eqn. [B.6]). For the third term, the following expansion must be simplified:

$$\begin{aligned} U_0\left[\left(-a_z^\dagger + a_z\right)\left(I_z\cos\Delta\omega t_1 + I_y\sin\Delta\omega t_1\right)\right]U_0^\dagger &= \left(-a_z^\dagger + a_z\right)\left(I_z\cos\Delta\omega t_1 + I_y\sin\Delta\omega t_1\right) \\ &+ \frac{it_0}{\hbar}\left[\tilde{H}_1^{(0)}, \left(-a_z^\dagger + a_z\right)\left(I_z\cos\Delta\omega t_1 + I_y\sin\Delta\omega t_1\right)\right] \\ &+ \frac{1}{2!}\left(\frac{it_0}{\hbar}\right)^2\left[\tilde{H}_1^{(0)}, \left[\tilde{H}_1^{(0)}, \left(-a_z^\dagger + a_z\right)\left(I_z\cos\Delta\omega t_1 + I_y\sin\Delta\omega t_1\right)\right]\right] \\ &+ \frac{1}{3!}\left(\frac{it_0}{\hbar}\right)^3\left[\tilde{H}_1^{(0)}, \left[\tilde{H}_1^{(0)}, \left[\tilde{H}_1^{(0)}, \left(-a_z^\dagger + a_z\right)\left(I_z\cos\Delta\omega t_1 + I_y\sin\Delta\omega t_1\right)\right]\right]\right] \\ &+ \text{.....}\,. \end{aligned} \quad [B.13]$$

After the commutators are evaluated using eqn. [B.4], the expansion can be expressed in a closed form:

$$U_0\left[\left(-a_z^\dagger + a_z\right)\left(I_z\cos\Delta\omega t_1 + I_y\sin\Delta\omega t_1\right)\right]U_0^\dagger = \left[I_z\left(-a_z^\dagger + a_z\right) + \frac{i\hbar t_o}{2}\gamma G\sqrt{\frac{\hbar}{2m\omega_z}}\right] \times \cos\Delta\omega t_1$$

$$+ \left[\left(-a_z^\dagger + a_z\right)\left(I_y\cos\Theta - I_x\sin\Theta\right) + t_o\gamma G\sqrt{\frac{\hbar}{2m\omega_z}}\left(I_x\cos\Theta + I_y\sin\Theta\right)\right] \times \sin\Delta\omega t_1 \ , \qquad \text{[B.14]}$$

where

$$\Theta = t_o\gamma G\sqrt{\frac{\hbar}{2m\omega_z}}\left(-a_z^\dagger + a_z\right) . \qquad \text{[B.15]}$$

Substituting eqn. [B.14] into [B.12] gives $\tilde{H}_z(t)$;

$$\tilde{H}_z(t) = \tilde{H}_z + \frac{\left(\hbar\gamma G t_o\right)^2}{4m}\left(1 + \cos\Delta\omega t_1\right) - i\gamma G t_o\sqrt{\frac{\hbar\omega_z}{2m}}\left[\left(-a_z^\dagger + a_z\right)I_z\left(1 + \cos\Delta\omega t_1\right)\right.$$

$$+ \gamma G t_o\sqrt{\frac{\hbar}{2m\omega_z}}\left(I_x\cos\Theta + I_y\sin\Theta\right)\sin\Delta\omega t_1$$

$$\left. + \left(-a_z^\dagger + a_z\right)\left(I_y\cos\Theta - I_x\sin\Theta\right)\sin\Delta\omega t_1\right] . \qquad \text{[B.16]}$$

Using the initial density operator given by eqn. [A.21] of Appendix A, and assuming a negligible initial axial energy, the expectation value of the axial energy in the proposed time-domain experiment (eqn. [B.2]) is

$$\begin{aligned} \langle E_z \rangle(t) &= Tr\left[\tilde{H}_z(t)\,\rho(0)\right] \\ &= \frac{(\hbar\,\gamma G\,t_0)^2}{4m}(1+\cos\Delta\omega\,t_1)\,. \end{aligned} \qquad \text{[B.17]}$$

The expectation value in eqn. [B.17] must be interpreted in the quantum mechanical two-state picture. It is related to the probability of each ion in the cloud either being accelerated to maximum energy,

$$E_z = \frac{(\hbar\,\gamma G\,t_0)^2}{2m}\,, \qquad \text{[B.18]}$$

or obtaining no net energy gain at all. For example, if $\cos\Delta\omega\,t_1 = 1$, then all ions (in the two internal states connected by the gradient field) are excited to the energy give by eqn. [B.18]. If $\cos\Delta\omega\,t_1 = 0$, then half of the ions are excited to this value while the other half are not excited at all. If $\cos\Delta\omega\,t_1 = -1$, then no ion is excited.

Appendix C: Parametric IRITE by Hexapolar Field Gradient

Any spatially inhomogeneous field can couple the internal eigenstates with the external translational motion of an atomic or a molecular system.[1] In the IRITE experiment proposed in Chapter 2, a quadrupolar gradient field is used (eqn. [2.1]). The effect of a hexapolar gradient field is examined in this appendix. There are two motivations for this analysis. One is to determine if a higher multipole gradient can be more effective in exciting the ions. The other is that often it is difficult to generate a field that is purely quadrupolar and without any higher components. This is the case, for example, in a microwave cavity necessary for microwave-frequency IRITE.[2] How this will effect the experiment needs to be examined.

The same rotating frame analysis used in the previous two appendices is utilized here. The only significant difference is that the change in the amplitude of oscillation, instead of the change in the energy, is analyzed. This will allow the parametric nature of hexapolar IRITE to be shown more clearly. Again, excitation of the axial oscillation is considered, but the results are applicable to the radial motions without notable change.

The axial hexapolar gradient is modeled as

$$E_z(t) = F z^2 \left[\cos(\omega_0 + 2\omega_z)t + \cos(\omega_0 - 2\omega_z)t\right] . \qquad [C.1]$$

Such a gradient would be useful for exciting the axial motion through a parallel ($\Delta M_J = 0$) transition. Choice of the frequencies will be explained later. Only the z-component of the field is relevant: Unless the cyclotron or the magnetron frequency happens to be same as the axial frequency, the x- and y-components do not effect the ion's motion. The corresponding perturbative Hamiltonian is

$$H_1 = \gamma F \left(I_z z^2 \right) \left[\cos(\omega_0 - 2\omega_z)t + \cos(\omega_o + 2\omega_z)t \right]. \qquad [C.2]$$

The spatial operator z^2 in the rotating frame defined by the unperturbed Hamiltonian (eqn. [A.7]) is

$$\begin{aligned} \tilde{z}^2 &= U^\dagger z^2 U \\ &= U^\dagger \left[\sqrt{\frac{\hbar}{2m\omega_z}} \left(a_z^\dagger + a_z \right) \right]^2 U \qquad [C.3] \\ &= \frac{\hbar}{2m\omega_z} \left[2a_z^\dagger a_z + 1 + a_z^{\dagger 2} \exp(-i2\omega_z t) + a_z^2 \exp(i2\omega_z t) \right]. \end{aligned}$$

Substituting eqn. [C.3] for z^2 and eqn. [A.10] for I_z in [C.2] gives the rotating frame Hamiltonian:

$$\tilde{H}_1 = \gamma F \frac{\hbar}{2m\omega_z}\left(2a_z^{\dagger}a_z + 1\right)\left(I_z \cos\omega_0 t - I_y \sin\omega_0 t\right)\left[\cos(\omega_0 - 2\omega_z)t + \cos(\omega_o + 2\omega_z)t\right]$$

$$+ \gamma F \frac{\hbar}{4m\omega_z}\left\{\left(a_z^{\dagger 2} + a_z^2\right)I_z\left[\cos(\omega_0 - 2\omega_z)t + \cos(\omega_o + 2\omega_z)t\right]\right.$$

$$+\left(a_z^{\dagger 2} + a_z^2\right)I_y\left[\sin(\omega_0 - 2\omega_z)t + \sin(\omega_o + 2\omega_z)t\right] \qquad \text{[C.4]}$$

$$-i\left(a_z^{\dagger 2} - a_z^2\right)I_y\left[\cos(\omega_0 - 2\omega_z)t - \cos(\omega_o + 2\omega_z)t\right]$$

$$\left.+\,i\left(a_z^{\dagger 2} - a_z^2\right)I_z\left[\sin(\omega_0 - 2\omega_z)t - \sin(\omega_o + 2\omega_z)t\right]\right\}$$

$$\times\ \left[\cos(\omega_o - 2\omega_z)t + \cos(\omega_o + 2\omega_z)t\right].$$

The choice of the field frequencies in eqn. [C.2] is justified here. The resulting time-averaged rotating frame Hamiltonian is

$$\tilde{H}_1^{(0)} = \frac{\gamma F \hbar}{4m\omega_z}\left(a_z^{\dagger 2} + a_z^2\right) I_z\,. \qquad \text{[C.5]}$$

The objective of calculation in this appendix is the time evolution of the axial spatial operator under the gradient field:

$$\tilde{z}(t) = \exp\left(i\,\tilde{H}_1^{(0)}\,t/\hbar\right)\tilde{z}\,\exp\left(-i\,\tilde{H}_1^{(0)}\,t/\hbar\right)$$

$$= \tilde{z} + \frac{i\,t}{\hbar}\left[\tilde{H}_1^{(0)}, \tilde{z}\right] + \frac{1}{2!}\left(\frac{i\,t}{\hbar}\right)^2\left[\tilde{H}_1^{(0)}, \left[\tilde{H}_1^{(0)}, \tilde{z}\right]\right] \qquad [C.6]$$

$$+ \frac{1}{3!}\left(\frac{i\,t}{\hbar}\right)^3\left[\tilde{H}_1^{(0)}, \left[\tilde{H}_1^{(0)}, \left[\tilde{H}_1^{(0)}, \tilde{z}\right]\right]\right] + \ldots\ldots .$$

The z-operator in the rotating frame was given previously (eqn. [A.11]):

$$\tilde{z} = \sqrt{\frac{\hbar}{2m\omega_z}}\left[\left(a_z^\dagger + a_z\right)\cos\omega_z t - i\left(a_z^\dagger - a_z\right)\sin\omega_z t\right]. \qquad [C.7]$$

The commutators in eqn. [C.6] are

$$\left[\tilde{H}_1^{(0)}, \tilde{z}\right] = \sqrt{\frac{\hbar}{2m\omega_z}}\,\frac{\gamma F\hbar}{2m\omega_z}\,I_z\left[a_z\exp(-i\omega_z t) - a_z^\dagger\exp(i\omega_z t)\right]$$

$$\left[\tilde{H}_1^{(0)}, \left[\tilde{H}_1^{(0)}, \tilde{z}\right]\right] = -\sqrt{\frac{\hbar}{2m\omega_z}}\left(\frac{\gamma F\hbar}{2m\omega_z}\right)^2 I_z^2\left[a_z^\dagger\exp(-i\omega_z t) + a_z\exp(i\omega_z t)\right] \qquad [C.8]$$

$$\left[\tilde{H}_1^{(0)}, \left[\tilde{H}_1^{(0)}, \left[\tilde{H}_1^{(0)}, \tilde{z}\right]\right]\right] = -\sqrt{\frac{\hbar}{2m\omega_z}}\left(\frac{\gamma F\hbar}{2m\omega_z}\right)^3 I_z^3\left[a_z\exp(-i\omega_z t) - a_z^\dagger\exp(i\omega_z t)\right]$$

$$\vdots$$

Inserting [C.8] into eqn. [C.6] and rearranging,

$$\tilde{z}(t) = \sqrt{\frac{\hbar}{2m\omega_z}}\left[a_z^\dagger \exp(-i\omega_z t) + a_z \exp(i\omega_z t)\right]\left[1 - \frac{1}{2!}\left(\frac{i\,t}{\hbar}\frac{\gamma F \hbar}{2m\omega_z} I_z\right)^2 + \ldots.\right]$$

$$+ \sqrt{\frac{\hbar}{2m\omega_z}}\left[a_z \exp(-i\omega_z t) - a_z^\dagger \exp(i\omega_z t)\right]\left[\frac{i\,t}{\hbar}\frac{\gamma F \hbar}{2m\omega_z} I_z - \frac{1}{3!}\left(\frac{i\,t}{\hbar}\frac{\gamma F \hbar}{2m\omega_z} I_z\right)^3 + \ldots.\right]$$

$$= \sqrt{\frac{\hbar}{2m\omega_z}}\left[a_z^\dagger \exp(-i\omega_z t) + a_z \exp(i\omega_z t)\right] \cdot \cosh\left(\frac{\gamma F t}{2m\omega_z} I_z\right) \qquad \text{[C.9]}$$

$$+ i\sqrt{\frac{\hbar}{2m\omega_z}}\left[a_z \exp(-i\omega_z t) - a_z^\dagger \exp(i\omega_z t)\right] \cdot \sinh\left(\frac{\gamma F t}{2m\omega_z} I_z\right).$$

Note that the factor in the first term,

$$\sqrt{\frac{\hbar}{2m\omega_z}}\left[a_z^\dagger \exp(-i\omega_z t) + a_z \exp(i\omega_z t)\right],$$

is equal to the initial z-operator in the rotating frame, $\tilde{z}$ (eqn. [C.7]);

$$\tilde{z}(t) = \tilde{z} \cdot \cosh\left(\frac{\gamma F t}{2m\omega_z} I_z\right) + i\sqrt{\frac{\hbar}{2m\omega_z}}\left[a_z \exp(-i\omega_z t) - a_z^\dagger \exp(i\omega_z t)\right] \cdot \sinh\left(\frac{\gamma F t}{2m\omega_z} I_z\right).$$

[C.10]

A somewhat different result is obtained if the gradient field is applied with a $\pi/2$ phase delay:

$$\vec{E}_z(\vec{r},\, t) = F\left(z^2\,\hat{k}\right)\left[\sin(\omega_0 + 2\omega_z)t + \sin(\omega_0 - 2\omega_z)t\right]. \qquad [C.11]$$

Then the average rotating frame Hamiltonian is

$$\tilde{H}_1^{(0)} = i\frac{\gamma F \hbar}{4m\omega_z}\left(a_z^{\dagger 2} - a_z^2\right) I_z \qquad [C.12]$$

and the resulting time-dependent axial operator is

$$\tilde{z}(t) = \sqrt{\frac{\hbar}{2m\omega_z}}\left[a_z^\dagger \exp(-i\omega_z t) + a_z \exp(i\omega_z t)\right]\cdot\cosh\left(\frac{\gamma F t}{2m\omega_z} I_z\right)$$

$$+ i\sqrt{\frac{\hbar}{2m\omega_z}}\left[a_z \exp(-i\omega_z t) - a_z^\dagger \exp(i\omega_z t)\right]\cdot\sinh\left(\frac{\gamma F t}{2m\omega_z} I_z\right)$$

$$= \tilde{z}\cdot\cosh\left(\frac{\gamma F t}{2m\omega_z} I_z\right) + \sqrt{\frac{\hbar}{2m\omega_z}}\left[a_z^\dagger \exp(i\omega_z t) + a_z \exp(-i\omega_z t)\right]\cdot\sinh\left(\frac{\gamma F t}{2m\omega_z} I_z\right).$$

[C.13]

Equations [C.10] and [C.13] give the same description of excitation by the hexapole field: Amplitude of the oscillation increases hyperbolically,

$$z(t) = z_0\cdot\cosh\left(\frac{\mu F t}{2m\omega_z}\right), \qquad [C.14]$$

where z_0 is the initial oscillation amplitude. This differs from IRITE using a quadrupolar gradient field, where the amplitude increases linearly in time. The second term in eqn. [C.13] indicates that ions that are 180 degrees out of phase in their oscillations are also excited. (The second term in eqn. [C.10] describes the role of initial momentum.) These properties are consistent with parametric excitations.[3,4] Note that since the cosine is an even function, the amplitude of oscillation can only increase, regardless of the initial internal state.

Using numbers comparable to the parameters discussed in Chapter 2 (eqn. [A.3]), with F = 2 kV/cm^3, $\omega_-/2\pi$ = 20 kHz, and t = 1 sec, $z(t = 1 \text{ sec}) = 1.1\, z_0$. With a large enough z_0, this amplitude change can be made greater than the ~ 4 mm increase expected for the quadrupolar excitation. However, there are experimental difficulties associated with a large initial amplitude. The most significant of these is the problem of obtaining a harmonic trapping potential over a large volume.[5] Since the magnitude of excitation is highly sensitive to the experimental parameters, it maybe possible to design an IRITE experiment in which the use of a hexapolar gradient field is advantageous. But for the experiment described in Chapter 2, a quadrupole field is more appropriate.

C.1 References

(1) Ramsey, N. F. *Molecular Beams*; Oxford University Press: London, 1956.

(2) Poole, Jr., C. P. *Electron Spin Resonance*, 2nd ed.; Wiley: New York, 1983.

(3) Landau, L. D.; Lifshitz, E. M. *Mechanics*, 3rd ed.; Pergamon Press: Oxford, 1976.

(4) Schweikhard, L.; Marshall, A. G. *J. Am. Soc. Mass Spectrom.* **1993**, *4*, 433.

(5) Brown, L. S.; Gabrielse, G. *Rev. Mod. Phys.* **1986**, *58*, 233.